An Experimental Investigation of Dechanneling in Copper Single Crystals

by

Paul V. G. Tulonen, hBSc., Brock.

A Thesis

submitted to the Department of Physics

in partial fulfilment of the requirements

for the degree of

Master of Science

January 1984

Brock University

St. Catharines, Ontario

© Paul V. G. Tulonen

Abstract

This investigation comprises a comparison of experimental and theoretical dechanneling of MeV protons in copper single crystals. Dechanneling results when an ion's transverse energy increases to the value where the ion can undergo small impact parameter collisions with individual atoms. Depth dependent dechanneling rates were determined as functions of lattice temperature, ion beam energy and crystal axis orientation. Ion beam energies were 1MeV and 2MeV, temperatures ranged from 35 K to 280 K and the experiment was carried out along both the $\langle 100 \rangle$ and $\langle 110 \rangle$ axes.

Experimental data took the form of aligned and random Rutherford backscattered energy spectra. Dechanneling rates were extracted from these spectra using a single scattering theory that took explicit account of the different stopping powers experienced by channeled and dechanneled ions and also included a correction factor to take into account multiple scattering effects along the ion's trajectory.

The assumption of statistical equilibrium and small angle scattering of the channeled ions allows a description of dechanneling in terms of the solution of a diffusion like equation which contains a so called diffusion function. The diffusion function is shown to be related to the increase in average transverse energy. Theoretical treatments of increase in average transverse energy due to collisions of projectiles with channel electrons and thermal perturbations in the lattice potential are reviewed. Using the diffusion equation and the electron density in the channel centre as a fitting parameter dechanneling rates are extracted.

Excellent agreement between theory and experiment has been demonstrated. Electron densities determined in the fitting procedure appear to be realistic. The surface parameters show themselves to be good indicators of the quality of the crystal.

Acknowledgements

The author would like to express his most sincere appreciation to Dr. J.A. Moore for supervising this thesis and Dr. L.M. Howe for participating in the experimental investigation and calculating the theoretical dechanneling rates.

The award of OGS fellowship and the financial assistance from NSERC is gratefully acknowledged.

My thanks to Mr. T. Quenneville for his technical help regarding the polishing of crystals; I also thank the institutions of Guelph University and Chalk River Nuclear Laboratories for allowing me access to their facilities.

I would like to express my appreciation to my spouse Rita and my family for their support and understanding throughout my studies.

Table of Contents

List of Tables

List of Illustrations

1. Introduction

MeV and keV ion beams can be used for analysing and modifying physical properties within several microns of a solid's[1-6] surface. Modifications may be affected through controlled implantation of ion species. For example: crystalline structure can be made amorphous and doping can be carried out in semiconductor manufacturing. Analyses can be performed using the ability to determine mass, concentration and location of atoms using the techniques of Rutherford backscattering (RBS), nuclear reactions and channeling. Atom location techniques, for example, require channeling of ions along major crystallographic axes of a single crystal and then the atom's position within the lattice can be deduced from the resultant spectra.

1.1 Background

Consider an ion beam incident upon a single crystal, with energy E_o, along a major crystallographic direction. To the beam, there appears an array of atomic strings parallel to the axis with end points being the surface atoms. To a first approximation the ion beam is assumed to interact with an infinite single string of atoms. An incident angle, ϕ, can be defined as that angle between the direction of the beam and crystallographic axis.

The approximation to the potential of a Thomas-Fermi, T-F, atom used by Lindhard[7] to derive an expression for the effective interaction between a single string and an ion whose trajectory is almost parallel to the string is given as

$$V(R) = \frac{Z1\ Z2\ e^2}{R} \left(1 - \left(1 + (Ca/R)^2\right)^{-\frac{1}{2}}\right) \qquad 1.1.1$$

Where Z1,Z2 are ion and lattice atom atomic numbers, R is the distance from a lattice atom, C is a constant with a value of $\sqrt{3}$, a is the T-F screening distance. By integrating equation 1.1.1 along the string's axis the standard continuum potential U(r) is obtained

$$U(r) = \frac{Z1\ Z2\ e^2}{d} \ln(1 + (Ca/r)^2) \qquad 1.1.2$$

Where d is the axial lattice spacing, and r is the radial distance perpendicular to the string. This can be looked upon as an averaging of the discrete spherical atomic charge distributions into a continuum with a cylindrically symmetric charge distribution.

Trajectories can be described by the standard continuum potential if an ion's trajectory at the channel centre with respect to the string is less than a critical angle defined as

$$\psi_1 = \sqrt{2\ Z1\ Z2\ e^2 / E\ d} \qquad 1.1.3$$

If not, the projectile may, through small impact parameter collisions with individual atoms in the string, undergo large angle scattering.

For ions under the influence of the potential U(r), their velocities parallel to the string are constant and it is thus necessary that energy in the direction perpendicular to the string, called the transverse energy, be conserved. Thus it is convenient to study the three dimensional motion of ions as a projection on a two dimensional plane perpendicular to the string. The parameter of interest now being the transverse energy, $E_\perp$, which can be calculated as follows

$$E_\perp = K_\perp + U(r) \qquad 1.1.4$$

Where $K_\perp$ is the transverse kinetic energy.

Ideally, two regimes of projectile energies can be defined with respect to the critical transverse energy $E_{\perp,c} (= \psi_1^2 E_0)$:

i...Channeled fraction

> Those projectiles with transverse energies less than the critical transverse energy; they are steered away from the string and will thus be precluded from small impact parameter/large angle scattering collisions.

ii...Random fraction

> Those projectiles with transverse energies greater than the critical transverse energy; they interact normally with the lattice and may undergo large angle scattering as a result of small impact parameter collisions.

In reality, a channeled ion scatters from thermally vibrating lattice atoms and individual electrons. In an individual collision an ion may scatter to higher or to lower transverse energy. Since the initial distribution is peaked towards low transverse energies it is expected that the transverse energy distribution will broaden and thus the average transverse energy of the beam will tend to increase with depth. Theoretically, the change in transverse energy distribution with depth is given by solving a diffusion-like equation. The corresponding changes to the transverse energies are controlled mainly by electron collisions within the channel and with thermally vibrating string nuclei. Due to these scatterings, a channeled ion's transverse energy can increase to the point where it makes a transition from the channeled to the random fraction, i.e. the ion is dechanneled. Once part of the random fraction, an ion interacts normally with the lattice and may therefore undergo large angle elastic scattering.

Experimentally, the increase in dechanneled fraction with depth may be observed using RBS techniques . For a well aligned beam/crystal axis system the increase in average transverse energy with depth, which brings increasing numbers of ions into the random fraction, is seen in a backscattered spectrum as an increase in the aligned yield with depth, figure 1.1. If an amorphous solid of the same material were used then the ions would interact normally with all atoms. The backscattered yield for an amorphous solid quickly rises to the bulk value in the surface region; the slight increase in yield with depth is partially due to the change in differential scattering cross section as a function of energy, figure 1.1.

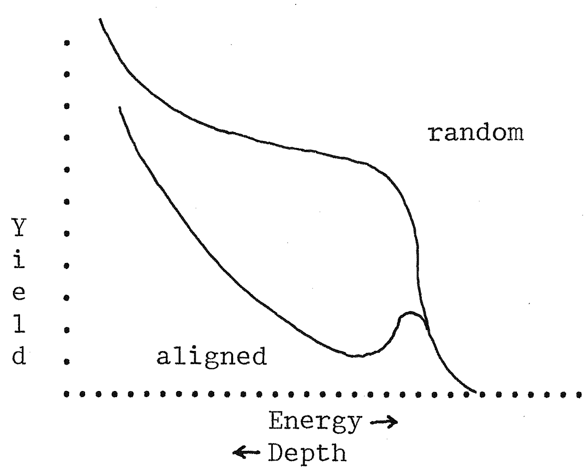

figure 1.1: schematic backscattered spectra

Dechanneled fractions can be extracted from these spectra and may then be compared with theoretically determined values.

1.2 Previous Work

In 1965 Lindhard[7] developed and used a continuum model to describe the net effect of scattering by electrons and atoms on channeled ions. This led to a diffusion-like equation whose solution describes the depth dependent transverse energy distribution for a group of projectiles. Since then several papers have been published dealing with significant improvements in treatment of nuclear and electronic scattering. Numerical solutions of the diffusion-like equation have led to theoretical determinations of the dechanneled fraction.

Thus far, experiment and theory have been investigated for silicon, germanium, tungsten and gold single crystals. Passing reference has also been made about iron, niobium, molybdenum and tantalum crystals as well.

In 1972 Bonderup et al[8], solving Lindhard's equations numerically, found that theoretical values for the dechanneled fractions were a factor of three lower than the experimental values for 1.6 MeV protons along the ⟨110⟩ axis of silicon at 20°C and 700°C. The authors knew that the nuclear and electronic scattering contributions were based on rather cursory estimates and likely needed modification.

In 1973 Shiott et al[9] modified equations in the previous paper by including a more realistic electron density in the channel centre and by taking into account terms in the nuclear scattering of higher order than Lindhard's first order analysis. Also in 1973 Pederson et al[10], based on Shiott's modifications, found the following: For both 1.6 MeV protons along the ⟨110⟩ axis of silicon and 2.0 MeV protons along the ⟨100⟩ axis of tungsten agreement was excellent at 20°C and deviated by up to 20% by the 700°C run. For several runs on tungsten down other axes they found good agreement. On iron, niobium, molybdenum and tantalum theoretical values were a factor of 1.5 to 2 lower. They suggested that this might be attributed to large concentrations of defects.

In 1980 Matsunami and Howe[11] treated the nuclear term in a slightly different manner by adding in a high transverse energy contribution[12] to Lindhard's first order term. The electronic term was modified by taking into account the geometry of the channel using a multi-string formulation, and by using the electron density at the channel centre as a fitting parameter. They found for both 1.6 MeV and 2.0 MeV protons in silicon and germanium respectively along the ⟨110⟩ and ⟨111⟩ axes that agreement with experiment was good with deviations of 10-20% at shallow depths and 10% at greater depths. These were performed at temperatures ranging from 293 K to 973 K.

In 1980 Moore[13] developed a method for analysing experimental data which took into account different rates of energy loss for channeled and random fraction ions, variation of stopping powers and stopping cross sections with energy and deviation of backscattered spectra from single scattering theory. In this method it has been recognized that there is no unique trajectory associated with the backscattered yield at a particular energy. By taking this into consideration better representations of experimental dechanneled fractions may be obtained.

Recently, 1983, Howe et al[14] applied the theoretical method of Matsunami and Howe[11] with the Moore[13] treatment of experimental spectra to the interpretation of gold dechanneling data. The results for 0.5-2.0 MeV protons along ⟨110⟩ axis at temperatures from 35 K to 275 K were that theory and experiment matched to within 10%.

1.3 Thesis Topic

This thesis will concern itself with the extraction of experimental and comparison with theoretical dechanneling rates for copper single crystals; estimates of electron densities in the channel centre for the two axes investigated will also result. The study comprises an investigation of the dependence of the dechanneled fraction on lattice temperature, ion beam energy and axial direction. The theoretical treatment will be based on the latest model of Matsunami and Howe[11] which treats dechanneling as a diffusion problem and which includes the electron density in the channel centre as a fitting parameter. The experimental data will be analysed using a method developed by Moore[13] which explicitly takes into account the different stopping powers experienced by channeled and dechanneled ions.

Given the fact that only the 1983 paper[14] has been investigated utilizing the more accurate treatment of experimental data it was felt that further investigations were necessary in order to extend the domain of validity of the theoretical model and treatment of the experimental data. Copper was chosen for it's availability as a high quality single crystal and the fact that it's dechanneling data has not been evaluated using the newest techniques. Copper has properties similar to but sufficiently different from those systems already studied, eg. atomic mass, debye temperature etc., that further dechanneling information may be useful when looking for trends.

2. Theoretical Dechanneling: Introduction

This chapter is an overview of dechanneling theory based on an analysis of the four most significant papers starting from Lindhard's[7] classic 1965 work to Matsunami and Howe's[11] research in 1980.

When the functional relationship of the depth-transverse energy distribution, $g(E_\perp, z)$, is known it becomes possible to extract the dechanneled fraction, $\chi(z)$, as a function of depth z. This is performed by integrating the product of this distribution with a nuclear scattering (also refered to as close encounter or small impact parameter) probability function, Υ, over transverse energy, we get the following

$$\chi(z) = \int dE_\perp g(E_\perp, z)\, \Upsilon(E_\perp) \qquad 2.\ .1$$

The close encounter nuclear scattering probability function approaches zero for well channeled ions and one for the random fraction; it can be approximated as a step function, written as

$$\Upsilon(E_\perp) = \begin{cases} 0 & E_\perp < E_{\perp,c} \\ 1 & E_\perp > E_{\perp,c} \end{cases} \qquad 2.\ .2$$

Thus, in this two beam model, the problem of calculating a dechanneled fraction is completely specified by the determination of the depth-transverse energy distribution function.

2.1 Dechanneling Theory

A beam of ions incident upon a crystal along a crystallographic axis will have an initial transverse energy distribution due to collimation, beam/axis alignment and impact parameter distribution. This distribution in phase space, however, will not be in statistical equilibrium.

For a perfectly collimated beam at zero depth the initial transverse energy distribution is given by

$$g(E_\perp,0)\ dE_\perp = d(r^2)\ /\ r_o^2 \qquad 2.1.0$$

Where r is the radius of the transverse unit cell area per string and can be defined with respect to atomic density, N, and axial lattice constant, d, as $\pi r_o^2 = 1\ /\ d\ N$ (overlap of unit cells being ignored). And, $E_\perp$ is equal to $E\phi^2 + U(r)$.

At zero depth, a group of particles on an energy shell $E_\perp$ to $E_\perp + dE_\perp$ has a real space distribution in the transverse plane as represented in figure 2.1 and a momentum space distribution as in figure 2.2.

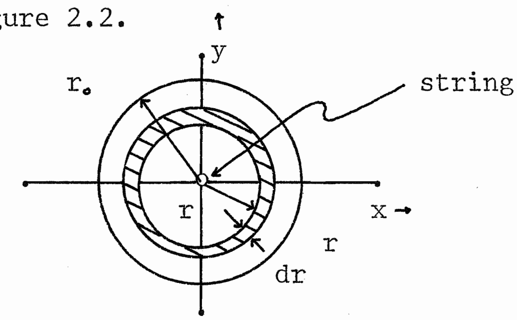

figure 2.1: real space distribution

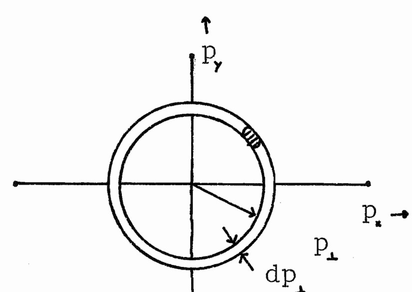

figure 2.2: momentum space distribution

As this group penetrates the crystal it would be expected that the phase space distribution would become modified due to successive scatterings from the continuum strings. Statistical mechanics suggests that an equilibrium distribution will be achieved.

By considering elastic scattering collisions of ions with strings, randomly distributed in the transverse plane, Lindhard[7] estimated the depth at which statistical equilibrium would be reached to be roughly 1000 atomic layers, or, after an energy loss of 1 to 10 keV.

For this group of particles, which have attained statistical equilibrium, what is their spatial distribution in the transverse plane?

This group of particles obeys a conservation equation in terms of the transverse energy, and is written as

$$E_{\perp} = p_{\perp}^{2} / 2m + U(r) \qquad 2.1.1$$

Corresponding to a point in transverse real space, the accessible area in transverse momentum space is $2\pi p_{\perp} dp_{\perp}$, where, using 2.1.1 we find

$$2\pi p_{\perp} dp_{\perp} = 2\pi m \, dE_{\perp} = \text{constant} \qquad 2.1.2$$

Hence, for particles in statistical equilibrium, each accessible point in real space is equally probable. Thus particles with transverse energy in the range $E_{\perp}$ to $E_{\perp} + dE_{\perp}$ are uniformly distributed across the accessible area in the transverse plane. The accessible area is given by $A(E_{\perp}) = \pi(r_0^2 - \hat{r}^2)$ and $\hat{r}$, the distance of closest approach, is given by $E_{\perp} = U(\hat{r})$.

Now introduced into this idealized system of elastic collisions between ions and the standard string potential is the realism of thermally vibrating lattice atoms along with electrons which act as scattering centres. These scatterings will have the effect of altering the transverse energy distribution of the beam as a function of depth.

At a point r in transverse real space, for a particle of energy $E_{\perp}$ which scatters into an interval $dE_{\perp}'$ about energy $E_{\perp}'$, the probability of scattering can be written as $p_r(E_{\perp}', E_{\perp})dE_{\perp}'$. The group of particles with transverse energy $E_\perp$, having reached statistical equilibrium, have an areal probability distribution that is independent of depth. Thus when averaging over the accessible area the probability of scattering from $E_\perp$ to $E_\perp'$, over a path length dz, will be independent of depth and can be written as $dz\, p(E_\perp', E_\perp)\, dE_\perp'$.

In this situation, an equation can be written from which the transverse energy distribution function, $g(E_\perp, z)$, can be extracted. The equation for the transverse energy distribution as a function of depth is written as

$$\begin{aligned} g(E_\perp,z)\, dE_\perp = {} & g(E_\perp, z-dz)\, dE_\perp \\ & + \text{probability flux in} \\ & - \text{probability flux out} \end{aligned} \qquad 2.1.3$$

In terms of the scattering probability, 2.1.3 can be written as

$$\begin{aligned} g(E_\perp,z)\, dE_\perp = {} & g(E_\perp, z-dz)\, dE_\perp \\ & + \int dE_\perp'\, g(E_\perp', z-dz)\, p(E_\perp, E_\perp')\, dz\, dE_\perp \\ & - \int dE_\perp\, g(E_\perp, z-dz)\, p(E_\perp', E_\perp)\, dz\, dE_\perp' \end{aligned} \qquad 2.1.4$$

Letting $dz \rightarrow 0$ yields

$$\frac{\partial g(E_\perp,z)}{\partial z} = \int dE_\perp' \left\{ p(E_\perp, E_\perp')\, g(E_\perp', z) - p(E_\perp', E_\perp)\, g(E_\perp, z) \right\} \qquad 2.1.5$$

Utilizing the fact that the scattering probability function is highly peaked towards very small values in energy transfer $\hat{E}_\perp = E_\perp' - E_\perp$, Bonderup et al[8] performed a Taylor series expansion on equation 2.1.5 with the final result being a diffusion-like equation, as shown below

$$\frac{\partial g(E_\perp,z)}{\partial z} = \frac{\partial}{\partial E_\perp} \left\{ D(E_\perp) \frac{\partial}{\partial E_\perp} \left(g(E_\perp, z) \right) \right\} \qquad 2.1.6$$

The factor $D(E_\perp)$, called the diffusion function, is given by

$$D(E_\perp) = \frac{1}{2} \int d\hat{E}_\perp \hat{E}_\perp^2 \tilde{p}(E_\perp, |\hat{E}_\perp|) \qquad 2.1.7$$

Where $\tilde{p}(E_\perp, |\hat{E}_\perp|)$ is the probability per unit energy per unit length of a particle undergoing an energy transfer $\hat{E}_\perp$ to or from energy $E_\perp$. Through this parameter information about the physical attributes of the scattering system are passed to the diffusion equation, 2.1.6.

Equations 2.1.6 and 2.1.7 apply to the case of small transverse energy since then accessible area is approximately a constant.

The diffusion function $D(E_\perp)$ is, physically, the mean square transverse energy transfer per unit length and it is a function of transverse energy, independent of transverse energy distribution and depth.

It might be expected that to determine $D(E_\perp)$ a knowledge of the transition probability as a function of both transverse energy and energy transfer would be required. However, it is possible to utilize the small angle scattering information implicitly available through the stopping power and which is well modeled theoretically for monoenergetic ions to determine the diffusion function.

Consider a group of channeled ions, energy $E_\perp^\circ$ at depth $z_\circ$, which are in statistical equilibrium and therefore uniformly distributed across the accessible area in the transverse plane. Their change in average transverse energy with depth can be written

$$\frac{\partial \bar{E}_\perp}{\partial z} = \int dE_\perp E_\perp \frac{\partial g}{\partial z} \qquad 2.1.8$$

$$= \int dE_\perp E_\perp \left(D' \frac{\partial g}{\partial E_\perp} + D \frac{\partial^2 g}{\partial E_\perp^2} \right)$$

Using integration by parts and the fact that g is essentially a delta function $g(E_\perp,z) = \delta(E_\perp - E_\perp^\circ)$ at depth z_0, we get

$$D(E_\perp^\circ) = \int_0^{E_\perp^\circ} dE_\perp \frac{d\bar{E}_\perp}{dz} \qquad 2.1.9$$

Where $d\bar{E}_\perp/dz$ is for a group of monoenergetic ions of transverse energy $E_\perp$ averaged over the accessible area. Thus the diffusion function can be determined directly from the rate of change in average transverse energy as a function of depth.

Therefore, since the diffusion function can be determined in terms of well modeled physical properties, as will be seen in the next section, it is thus possible to determine the transverse energy distribution as a function of depth. One method of solving equation 2.1.6 for g is through a numerical technique such as a finite difference method. The rest of this chapter is concerned with various approaches used to determine the rate of change in the average transverse energy with depth.

If one assumes that nuclear (n) and electronic (e) contributions are independent functions of energy then the rate of change of average transverse energy with depth can be written as a linear combination of each term, this is written as

$$\frac{d\bar{E}_\perp(E_\perp)}{dz}_{a} = \frac{dE_\perp(E_\perp)}{dz}_{n,a} + \frac{dE_\perp(E_\perp)}{dz}_{e,a} \qquad 2.1.10$$

Where subscripts a,n and e stand for aligned, nuclear and electronic respectively.

Equations in the remainder of the thesis will be expressed in either transverse energy, $E_\perp$, or in reduced transverse energy, $\varepsilon_\perp = 2\,E_\perp/\psi_1^2 E$, formats.

2.2 Increase in Average Transverse Energy: Nuclear Component

Lindhard's[7] treatment (which should be consulted by the serious reader) of the nuclear scattering contribution to the increase in average transverse energy of the channeled fraction consists of summing momentum transfers to beam ions due to collisions with thermally displaced lattice atoms. Displaced atoms create a perturbation in the continuum string potential resulting in a force fluctuation, $d\vec{F}$, experienced by passing ions, figure 2.3.

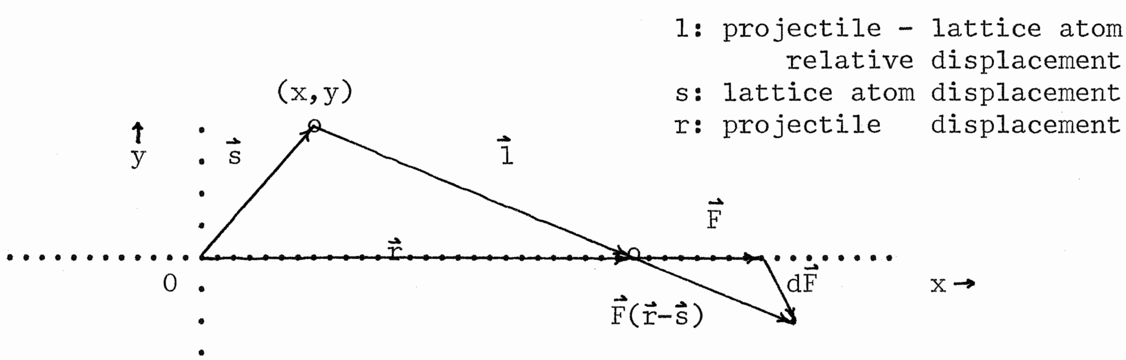

figure 2.3: Geometry of displaced lattice atom relative to the string and the passing ion, from Shiott 1973.

When averaged over accessible area and thermal displacement of lattice atoms the fluctuations become proportional to the change in average transverse energy, written as

$$(d\bar{\varepsilon}_\perp/dz)_{n,a} = d^3 \psi_1^3 \langle d\vec{F}^2 \rangle / (2\ Z1\ Z2\ e^2)^2 \qquad 2.2.1$$

The two dimensional thermal vibration amplitude distribution is assumed to be gaussian with an RMS value of ρ .

Equation 2.2.1 is a function of $\varepsilon_\perp$ as a consequence of averaging over the accessible area, $A(\varepsilon_\perp)$. When averaging over the accessible area a uniform distribution resulting from statistical equilibrium is assumed.

The result is expressed in terms of a nuclear reduction function

$\gamma_{n,L}$, which is given by the ratio of the increase in average transverse energy for the channeled and random beams, given as

$$(d\bar{\varepsilon}_\perp/dz)_{n,a} = (d\bar{\varepsilon}_\perp/dz)_{n,r} \cdot \gamma_{n,L}(\varepsilon_\perp) \qquad 2.2.2$$

The increase in average transverse energy for the random beam is proportional to the theoretical random nuclear (nr) stopping power, written as

$$(d\bar{\varepsilon}_\perp/dz)_{n,r} = -(M1/M2)(d\varepsilon/dz) \qquad 2.2.3$$

Where the subscript r stands for the random system and M1 and M2 are the masses of the projectile and target atom respectively.

$\gamma_{n,L}(\varepsilon_\perp)$ evaluated to first order in s/r, the ratio of displacements of lattice atom and projectile relative to lattice position, yields

$$\gamma_{n,L}(\varepsilon_\perp) = \frac{1}{Ln}\,\frac{\rho^2}{(Ca)^2}\,\frac{1}{2}\,(1 - e^{-\varepsilon_\perp})^3\,(\frac{2}{3} + e^{\varepsilon_\perp}) \qquad 2.2.4$$

Where Ln is logarithmic and is derived from nuclear stopping power energy loss considerations.

In this formulation, for energies approaching the critical transverse energy, ie. $s/r \rightarrow 1$, the expansion becomes questionable; $\gamma_{n,L}(\varepsilon_\perp)$ is an order of magnitude smaller than the true value, in the most important region, where nuclear scattering dominates.

The paper by Shiott et al[9] addresses the above deficiency. They examined the next highest contributing order in s/r in the expansion of the force fluctuation from the continuum string and exact results for two other central forces. From this, they decided to modify the first order reduction function by requiring it to asymptote to unity at approximately the critical transverse energy. This was accomplished by including and adjusting the fitting parameter f in the following equation

$$\gamma_{n,S}(\varepsilon_\perp) = \frac{1}{Ln}\,\frac{\rho^2}{(Ca)^2}\,\frac{1}{2}\,(1 - e^{-\varepsilon_\perp})^3\,(\frac{2}{3} + e^{f\varepsilon_\perp}) \qquad 2.2.5$$

In contrast to Schiott, Matsunami and Howe[11] in the latest paper treat nuclear scattering at transverse energies approaching the critical value in terms of a quantum theoretical description given by Kitagawa and Ohtsuki.[12] The reduction function can consequently be written as

$$\chi_{n,L}(\varepsilon_\perp) + \chi_{n,K}(\varepsilon_\perp) = \frac{1}{2\,\mathrm{LnCn}} \quad \frac{\rho^2}{3\,a^2}(1 - e^{-\varepsilon_\perp})^3 \left(\frac{2}{3} + e^{\varepsilon_\perp}\right) \qquad 2.2.7$$

$$+ \exp\left(-\frac{3a^2}{\rho^2} \quad \frac{1}{(1+\varepsilon_\perp^{\circ})e^{\varepsilon_\perp} - 1}\right)$$

Where Cn is a correction factor such that contributions from large angle scatterings are excluded. The restriction is made since the model is one where the diffusion process is being exploited. This is accomplished by limiting scattering trajectories to those in the channeled fraction that remain channeled. The term $\varepsilon_\perp^{\circ}$ is equal to $3\ a^2 / r_o^2$; $\chi_{n,k}(\varepsilon_\perp)$ is the reduction function of Kitagawa and Ohtsuki.

2.3 Increase in Average Transverse Energy: Electronic Component

In Lindhard's[7] treatment the electron scattering contribution to the increase in average transverse energy of the channeled beam is normalized to the random nuclear scattering component. In order that all formulations are in the same units the results will be normalized to the random electronic component.

For an amorphous solid, ie. a random distribution of nuclei, the electron distribution can be considered to be uniform with average electron density ρ_o equal to Z2 N. For this case, the change in average transverse energy for the random electronic component can be written as

$$\frac{d\bar{\varepsilon}_\perp}{dz}_{e,r} = \frac{m}{2\ M1} \frac{d}{Z1\ Z2\ e^2}\ Se\ \rho_o \qquad 2.3.1$$

Where Se is the theoretical stopping cross section per electron for high velocity incident ions. Increase in average transverse energy can be attributed to the increase in average square fluctuation in angle from momentum transfers due to individual projectile-electron collisions. The term m is the electron mass.

For an aligned beam, the uniform distribution of electrons must be replaced by the cylindrically symmetric electron density $\rho(r)$ consistent with the standard continuum potential, ie. a single string model. From statistical equilibrium, projectiles will be distributed with equal probability over their accessible areas. Thus, evaluation of the aligned electronic term requires an averaging, $\langle ... \rangle$, over the accessible area and is written as

$$\frac{d\bar{\varepsilon}_\perp}{dz} = \left\langle \frac{m}{2\ M} \frac{d}{Z1\ Z2\ e^2}\ Se\ \rho(r) \right\rangle \qquad 2.3.2$$

The result of the above mentioned derivation can be formulated in terms of a reduction function, given by

$$(d\bar{\varepsilon}_\perp/dz)_{e,a} = (d\bar{\varepsilon}_\perp/dz)_{e,r} \cdot \gamma(\varepsilon_\perp) \qquad 2.3.3$$

The reduction function for the electronic term is thus the ratio of the aligned to random electronic increase in average transverse energy and is shown below

$$\gamma_{e,\perp}(\varepsilon_\perp) = (1 - e^{-\varepsilon_\perp}) \qquad 2.3.4$$

For this derivation the stopping cross section per electron, Se, has been assumed to be independent of electron density and is proportional to the logarithm of the ratio of maximum energy transfer divided by average ionization energy per atom, Le = $\log(2mv^2/I_o)$, I_o is approximately Z2 * 10 eV.

Bonderup et al[8] instead of using the average ionization energy, as Lindhard did for Le, used a form originally derived by Lindhard[15] from a dielectric approach, written as

$$Le = \log(2 m v^2 / \hbar \omega) - 1 \qquad 2.3.5$$

Now, when averaging over accessible area the additional term ω, $= (4\pi \rho e^2 / m)^{1/2}$, the classical resonant frequency, must be taken into account because of the added dependence on electron density. The reduction function now evaluates to

$$\gamma_{e,B}(\varepsilon_\perp) = (1 - e^{-\varepsilon_\perp})(1 + \frac{\alpha}{Le} \ln(\frac{1}{1 - e^{-\varepsilon_\perp}})) \qquad 2.3.6$$

This formulation gives the same result for energies approaching the critical transverse energy but modifies the contribution from the channel centre for low transverse energy ions. α is a function weakly dependent on $\varepsilon_\perp$.

Shiott et al[9] modified the previous paper's method by correcting for the fact that electrons outside a radius r_o had been neglected in averaging over the accessible area. They kept the standard electron density out to a radius r_c and then set the electron density to a constant ρ_o outside of this radius so that the total number of electrons per target nucleus would equal the atomic number Z2. r_c is approximately $r_o / \sqrt{2}$. The reduction function can then be written as

same as 2.3.6. $\qquad r < r_c$ or $\varepsilon_\perp > U(r_c)$

$$2.3.7$$

$$\gamma_{e,S}(\varepsilon_\perp) = \frac{\rho_o}{N\ Z2} \frac{(Le - 1)}{Le} \qquad r > r_c \text{ or } \varepsilon_\perp < U(r_c)$$

Matsunami and Howe's treatment[11], though similar to Shiott et al's[9], introduces a significant improvement into the continuum string model description of the electronic scattering contribution to increase in average transverse energy. This is accomplished by summing the standard electron density contributions from neighbouring strings in order to estimate the average electron density in the channel centre. Since the resulting electron density in the channel centre is approximately constant they divided the transverse real space into two regions. These regions are the channel centre, where a constant electron density is assumed, and string region, where the electron density is well described by the standard continuum potential electron density. The electron density in the channel centre is estimated using a multi-string formulation which partially takes into account the geometery of the channel. Recognizing that use of the standard charge density at these large distances may not necessarily be a good representation, in practice they use the constant electron density as a fitting parameter when fitting the theoretical dechanneling curves to experimental curves. The starting point is normally then the value determined for the standard electron density. Their formulation of the reduction function, once this is taken into consideration, can be written as

$$\gamma_{e,M}(\varepsilon_\perp) = \alpha'(1-e^{U_t-\varepsilon_\perp})(1-\frac{1}{CeLe}\ln(1-\frac{e^{\varepsilon_\perp}}{1+\varepsilon_\perp^{o}})) + \gamma_e^{o} \qquad r \leqslant r_t \text{ or } \varepsilon_\perp \geqslant Ut \qquad 2.3.8$$

$$\gamma_{e,M}(\varepsilon_\perp) = \gamma_e^{o} = \rho_o(Le - 1)/\ N\ Z2\ Ce\ Le \qquad r > r_t \text{ or } \varepsilon_\perp < Ut$$

Ut is the potential at which the transition from the channel centre to the string region occurs, Ce is a equal to (Le-1) / Le and α' is given approximately by $1 - \gamma_e^o$. One important feature of Matsunami and Howe's[11] treatment is that their formulation yields an analytic equation for the diffusion function which greatly facilitates the evaluation of the diffusion - like equation.

2.4 Comparison of Reduction Function Components

Figure 2.4 exhibits the relative sizes of the various reduction function components for protons on copper at 56 K , figure 2.4.

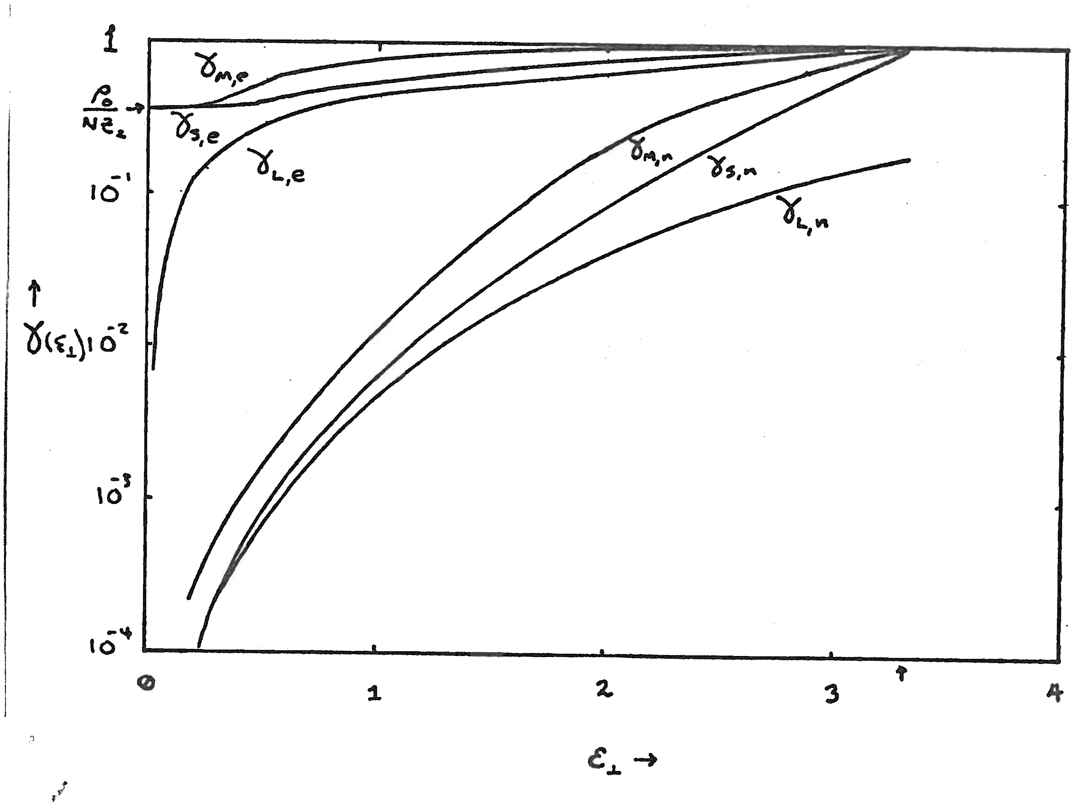

figure 2.4: comparison of reduction function components

When comparing the relative influences of the terms the electronic reduction function must be divided by Le/(2 Ln Z2), which here evaluates to 195. This is due to the fact that the electronic term must be renormalized to the random nuclear increase in average transverse energy. Thus the electronic term dominates the diffusion process for reduced transverse energies from zero up to approximately one; the nuclear term predominates for energies above one.

It is thus now easy to see why Bonderup et al[8]'s solution of Lindhard[7]'s reduction functions resulted in such a poor fit to experimental data. The electronic reduction function decreases unphysically to zero for zero transverse energy; this will result in a much too slow increase in transverse energy for well channeled ions. The nuclear reduction function does not reach the value that would be expected for ions in the random fraction; this results in a great decrease in diffusion for large transverse energy ions. These flaws can be seen to have been corrected for both reduction functions in the equations of Shiott et al[9] and Matsunami and Howe[11] and thus it can be appreciated why these formulations better describe experimental dechanneling fractions. Matsunami and Howe[11]'s nuclear reduction function, at low transverse energy, differs from Lindhard's due to the nuclear correction factor Cn. Also, Matsunami and Howe[11]'s electronic reduction function differs from Shiott et al[9]'s due to the term Ce. Shiott et al[9]'s and Matsunami and Howe[11]'s theoretical dechanneled fractions both agreed with experiment up to 1980. The agreement between theory and experiment is very good when Matsunami and Howe[11]'s treatment is combined with Moore[13]'s analysis of the experimental data.

3. Experimental Dechanneling: RBS Background

The experimental investigation of dechanneling in copper single crystals was carried out using Van de Graaff accelerators at Chalk River Nuclear Laboratories and Guelph University. The raw data was the yield of ions backscattered and measured as a function of energy using a solid state detector, figure 3.1. The solid state detector can be considered to be 100% efficient and it has an energy resolution of about 10 keV which translates to a depth resolution of 0.1 um for 1 MeV protons on copper. The solid angle subtended by the detector is approximately 0.01 steradians.

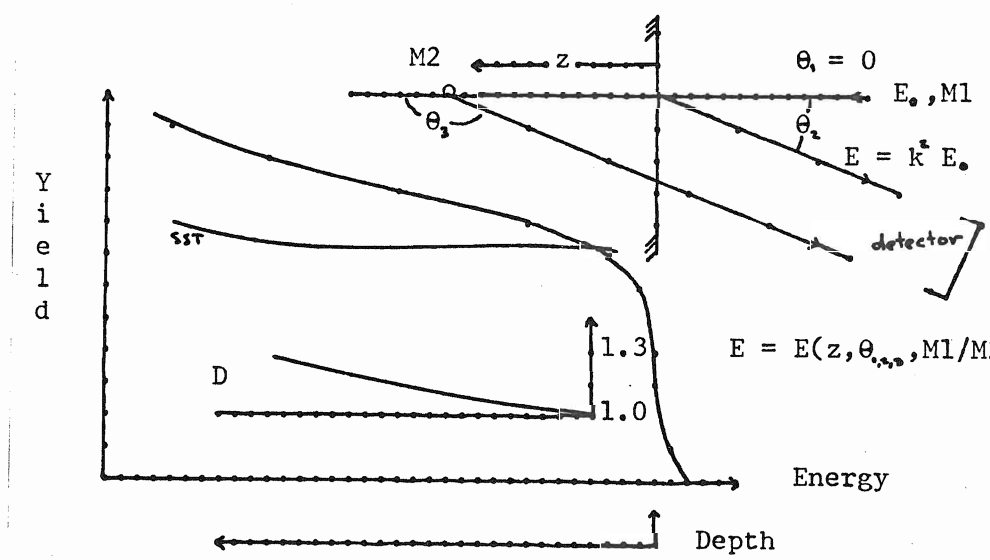

figure 3.1: random and single scattering theory yields, backscattering geometry, plural scattering

Converting an energy axis to a depth scale requires the knowledge of energy losses experienced by ions interacting with the lattice atoms. For ions that backscatter from a target atom, the ratio of kinetic energies after and before the collision yield the kinematic factor k^2 , written as[5]

$$k^2 = \left\{ \frac{(1-(M_1/M_2)^2 \sin^2\theta_3)^{1/2} + (M_1/M_2)\cos\theta_3}{1 + M_1/M_2} \right\}^2 \qquad 3.\ .1$$

Thus, the energy of an ion that backscatters from the surface is given by $E = k^2 E_0$. Those ions that backscatter at depth also lose energy due to inelastic multiple scattering along their ingoing and outgoing paths. Semi-empirical tabulations for the rate of energy loss, S(E), exist[16,17]; from this data an energy-depth relationship can be calculated using the following equations

ingoing $E_1 = E_0 - S(E_0)\, dz / \cos\theta_1$

$E_i = E_{i-1} - S(E_{i-1})\, dz / \cos\theta_1$

outgoing $E_{i-1} = k^2 E_i - S(k^2 E_i)\, dz / \cos\theta_2$

$$E_i' = \ldots(E_{i-2} = (E_{i-1} - S(E_{i-1})\, dz / \cos\theta_2)) \qquad 3.\ .2$$

This assumes that the stopping power is constant over each slab (shown in figure 3.2); precision will increase for thinner choices of slab thickness.

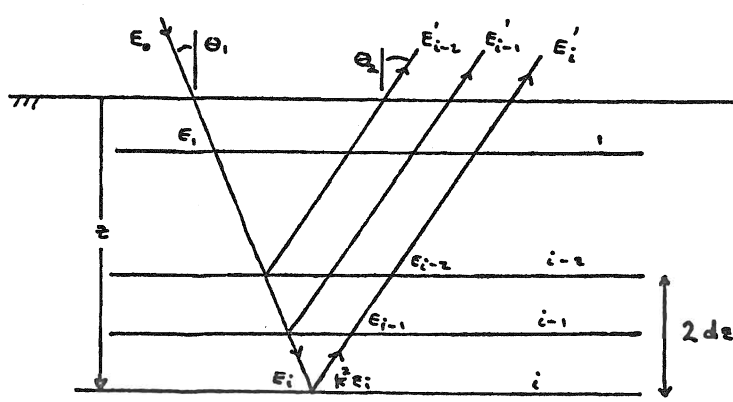

figure 3.2: energy-depth slab diagram

Therefore it can be seen that the random yield can be associated with both an energy and depth scale as in figure 3.1. Using a single scattering theory[13] and scattering cross section the theoretical yield for particles scattering through an angle θ_3 can be calculated. In this formulation the Rutherford scattering cross section has been corrected for deviations due to screening from orbital electrons[6]. The cross section is written as

$$\sigma(E) = F(E)\sigma_R(E) = \left(1-\frac{.049\ Z1\ Z2^{4/3}}{E}\right)\left\{\frac{Z1\ Z2\ e^2}{4E\ \sin^2(\theta_3\ /\ 2)}\right\}^2 \quad 3.\ .3$$

Figure 3.1 shows a comparison of the normalized single scattering and experimental yields. The inset graph, curve D, is the ratio of these curves and indicates the contribution to the experimental data due to multiple small angle/ plural large angle scattering. For 1 MeV protons on copper the effect rises to about 25% at 3.5 um. When the ion beam is well aligned with a major crystallographic direction an aligned spectrum results, figure 1.1. The suppressed yield, behind the surface peak, is a result of a decrease in nuclear scattering probability.

A comparison between the aligned and random spectra will allow a determination of the dechanneled fraction.

3.1 Conceptual Basis for Data Analysis

Ions with sufficiently large transverse energies, such that they are not bound by the coulomb barrier of the channel and therefore interact normally with the lattice, are said to be dechanneled and are thus part of the random fraction. These ions experience a stopping power equivalent to that experienced by ions traversing an amorphous solid. In contrast, the stopping power experienced by channeled ions is reduced compared with that experienced by ions in the random fraction. This is due to the fact that projectiles in the channel centre interact almost solely with channel electrons with the effect of the nuclei gradually increasing as the string is approached. In the amorphous system a projectile interacts more or less in a constant manner with a random array of nuclei and their electron distributions. In the aligned single crystal case, due to the different stopping powers, it is easy to imagine a family of trajectories for which the emergent energy, after backscattering, will be constant. These paths form a continuum with end members illustrated by paths a and c in figure 3.3. In path a ions dechannel at the surface; in path c ions dechannel and immediately backscatter at maximum depth for the emergent energy of interest.

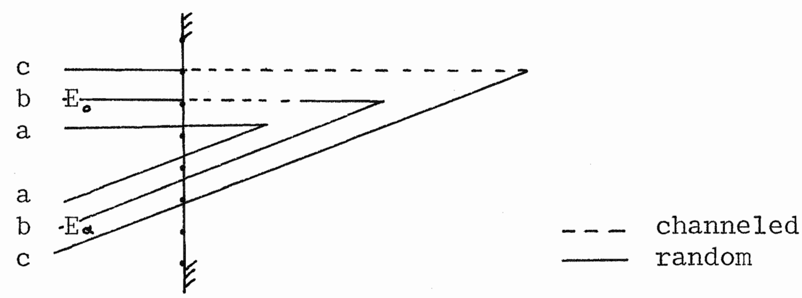

figure 3.3: trajectories with constant emergent energy

It must also be kept in mind that single scattering is only true for ions backscattered at the surface and, in a sense, at the point of maximum depth. All other ions in the random fraction of the beam will undergo multiple small angle/ plural large angle scattering to a certain degree.

Thus, the fact that there is no unique trajectory associated with a particular emergent energy and, also, that the ions actually undergo multiple small angle/ plural large angle scatterings must be taken into account when extracting the dechanneled fraction in an analysis of the aligned and random spectra.

3.2 Extraction of the Dechanneled Fraction, $\chi(z)$

For an amorphous solid a simple proportionality can be written for the backscattered yield as a function of fluence, I, solid angle subtended by the detector, $d\Omega$, target layer thickness, dz, and the atomic density n, this is given by

$$Y \propto I \; n \; d\Omega \, dz \qquad 3.2.1$$

The constant of proportionality is called the scattering cross section, σ_R. Rewriting equation 3.2.1 in terms of yield per unit energy gives

$$y = I \; n \; d\Omega \, dz \, \sigma_R \, / \, dE_1 \qquad 3.2.2$$

Since σ_R varies as $1 / E_r^2$, 3.2.2 can be rewritten as

$$y = K n I \; dz \; / \; E_r^2(z) \, dE_1 \qquad 3.2.3$$

Where K is a constant. Figure 3.4 illustrates the parameters.

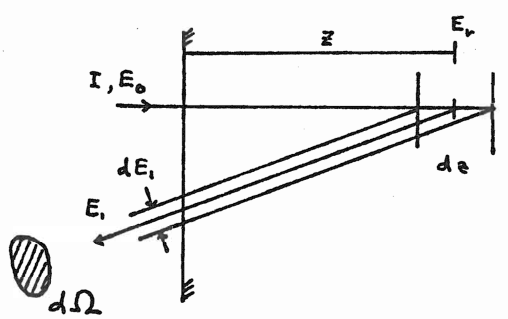

figure 3.4: random yield parameters

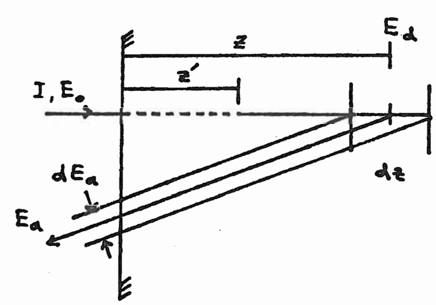

figure 3.5: aligned yield parmeters

For an aligned beam an added feature is that backscattering can not occur unless an ion has made a transition to the random fraction, figure 3.5, the rate of transition as a function of depth is $d\chi(z')$. Thus equation 3.2.3 when written in terms of the random yield for the single scattering theory evaluated at the surface yields the following equation

$$y(E_\alpha) = y_{r,o}\ E_o^2\ [S_{r,o}] \sum_i dz\ \ d\chi(z_i') \ /\ E_d^2 dE_a(z_i') \qquad 3.2.4$$

Where $[S_{r,o}]$, the surface channel stopping power factor, is given by

$$[S_{r,o}] = k^2 S_r(E_o)/\cos\theta_1 + S_r(k^2 E_o)/\cos\theta_2 \qquad 3.2.5$$

The sum is over all pairs of depths z & z', $z' < z$, such that the emergent energy is E_α.

Two cases should be considered in order to take into account the multiple small angle/ plural large angle scattering correction, D :

i... for an ion that backscatters immediately after dechanneling at maximum depth there can be only one large angle scattering event (a D factor of one).

ii... for an ion that dechannels at the surface the D factor is the ratio of the random to single scattering theory yields, inset graph in figure 3.1.

As it has not been attempted, to date, to model the multiple/ plural scattering for path combinations between these extremes, a linear approximation of the variation between these end members has been assumed.

The aligned yield can now be expressed in terms of the single scattering theory formulation taking into account the multiple/ plural scattering factor, $D_{z_i'}(E_\alpha)$, at a particular energy as shown below

$$y(E_\alpha) = y_{r,o}\ E_o^2\ [S_{r,o}]\sum_i dz\ d\chi(z_i')\ D_{z_i'}(E_\alpha)/E_d^2 dE_a(z_i') \qquad 3.2.6$$

Variation in $E_d^2 dE_\alpha$ for rechanneled ions has been neglected since it would be computationally difficult to take into account.

Equation 3.2.6 is the formulation by which the experimental data have been reduced and it is the same as that originally derived by

Moore[13]. By inverting this equation successive dechanneled fraction contributions, $d\chi_i$, starting from the surface slab can be calculated. Summing the individual terms, as a function of depth, will yield the dechanneling fraction $\chi(z)$.

3.3 Main Computer Program Description

Yield versus backscattering energy data for both the random and aligned spectra are averaged over a suitable interval, say 5 channel widths, starting just behind the surface peak. This data is then entered into the main program where channel numbers are converted into energies using the energy width per channel and the proper zero channel offset. Along with this data is entered the initial beam energy, the beam's fluence, the beam/target/detector system geometry, total number of data points and the channeled/random stopping power ratio The spectra are normalized using the ratio of the fluences. The kinematic factor is evaluated. Also calculated is the surface channel stopping power factor, equation 3.2.5.

With respect to the family of calculated curves which would be generated in an evaluation of the denominator in equation 3.2.6 it was decided that, since they are approximately linearly spaced functions of depth, an interpolation scheme would be used to generate the values. Thus two curves would be determined and the rest would be interpolated. These are (1) the envelope of the end points of the family of curves corresponding to backscattering immediately after dechanneling and (2) the curve corresponding to dechanneling at the surface, schematically shown in figure 3.6.

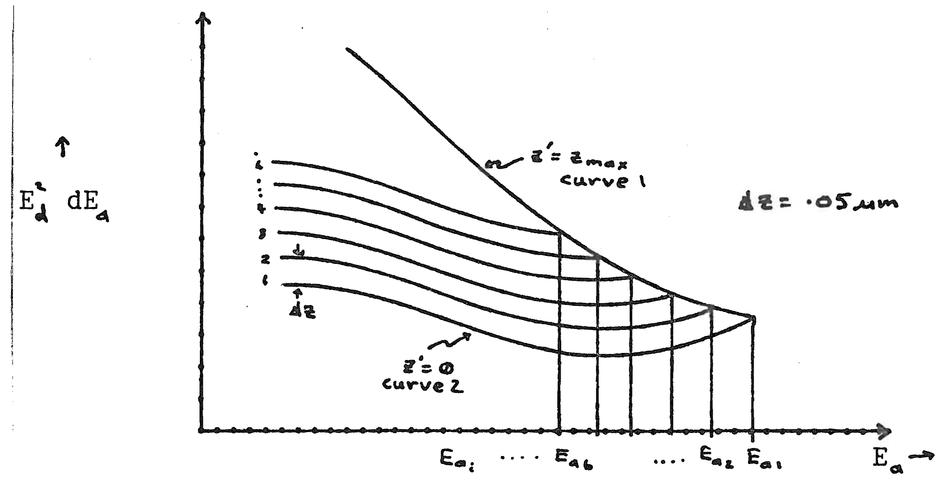

figure 3.6: interpolation scheme for $E_d^2 dE_a$

Also, the multiple/ plural scattering contribution is evaluated assuming a linear interpolation between the two end members enumerated in the cases considered in section 3.2. These are determined at energies corresponding to the discrete data points and incorporated into two matrices.

Starting just behind the surface peak, the contribution of each layer to the dechanneled fraction is determined. For the first layer there is only one contribution, written as

$$d\chi_1 = y(E_{a1})\, E_d^2\, dE_a(z_1') \,/\, y_{r,0}\, E_0^2 [S]_{r,0}\, D_{z_1'}(E_{a1})\, dz \qquad 3.3.1$$

In the next layer the contribution from the first layer is subtracted and then the rest is attributed to the change in dechanneled fraction of this layer, given by

$$d\chi_2 = \left\{ \frac{y(E_{a2})}{y_{r,0}\, E_0^2 [S]_{r,0}} - \frac{dz\, D_{z_1'}(E_{a2})\, d\chi_1}{E_d^2\, dE_a(z_1')} \right\} \frac{E_d^2\, dE_a(z_2')}{D_{z_2'}(E_{a2})\, dz} \qquad 3.3.2$$

This process is then continued for all the rest of the data.

Next, the changes in dechanneling fraction in each layer are summed to yield the dechanneling fraction as a function of depth. Graphs of the experimental dechanneling fractions are shown in chapter 5.

4. Crystal Quality: Introduction

Before extraction of dechanneling rates from aligned and random spectra, for this thesis, it is necessary to ensure that high-quality single crystals are being used. In this chapter preliminary results from Guelph University, taken to test the preparation techniques, will be used in evaluating the quality of the crystals.

4.1 Crystal Preparation

An attempt was made to evaluate the significance of defects in the bulk by comparing X-ray patterns before and after annealing. One crystal was vacuum annealed just below the melting point for 72 hours and then the temperature was decreased by 10°C per hour back to room temperature. This procedure should reduce the overall number of mobile defects.

Surface preparation just prior to channeling was needed in order to remove oxides from the exposed surface and any defects in the near surface region due to implantation of protons and helium ions during previous runs. Crystals were cleaned by mechanical-polishing with a .05 um alumina slurry on cloth for several minutes followed by a few minutes electro-polishing in a solution of 55% phosphoric acid and 45% distilled water at 1.6V potential. These techniques removed roughly 0.03 and 3 um of copper per minute respectively. Polishing was performed in air and it is expected that a slight reoxidation will occur before the crystals can be introduced into the vacuum.

4.2 Crystal Quality Data

Laue X-ray diffaction patterns were examined prior to and after annealing. There were no discernible differences between Laue patterns for the same crystal slice before and after annealing and when compared to slices from the same crystal and another crystal. A couple of Laue spots appeared to have some internal structure which may be indicative of a little strain.

A small digression is necessary here before proceeding to the rest of the data.

Backscatter spectra yield useful information for determining crystal quality when the ion beam is brought into close coincidence with a major crystallographic direction. Three parameters which will be investigated are the axial half angle, $\psi_{1/2}$, minimum yield, χ_{min}, and surface peak yield.

Their definitions and diagramatic representations follow:

$\psi_{1/2}$: the angle at full width half minimum of the channel dip, figure 4.1.

χ_{min} : ratio of the minimum in the aligned yield divided by the random yield, figure 4.1 and 4.2.

surface peak : yield associated with backscattering from atoms in the surface region, figure 4.2, shaded area.

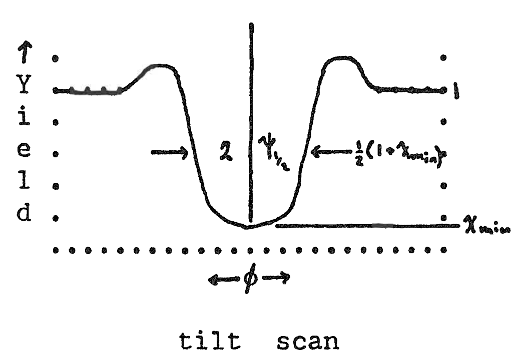

figure 4.1: angular dip spectrum

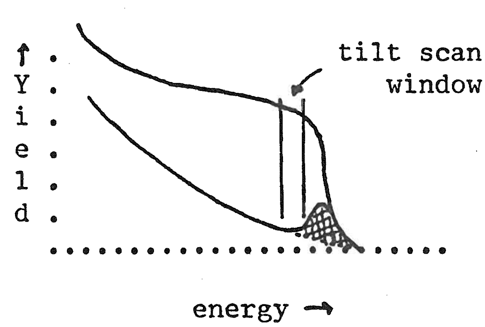

figure 4.2: aligned/random spectra

These parameters are functions of crystal structure and temperature and are sensitive to perfection of the lattice. They have been investigated experimentally and through computer simulations.

The following analysis is based on equations originally derived by Barrett,[18] using a computer simulation, as recorded in the Ion Beam Handbook.[19]

Axial half angles can be estimated through the following equation

$$\psi_{1/2} = 0.8\, F_{RS}(\xi)\, \psi_{1,B} \qquad 4.2.1$$

Barrett's characteristic angle, $\psi_{1,B}$, is given by $0.307\,(Z1\ Z2\ e^2/E\ d)^{1/2}$; $(Z1\ Z2\ e^2/d)$ is a measure of the strength of the string's potential energy barrier; it's strength increases with a decrease in atomic spacing along the axial direction. ξ is equal to $1.2\ u_1/a$, the Thomas- Fermi screening radius, a, equals $.8855\ a_0\,(Z1^{1/2} + Z2^{1/2})^{-2/3}$ and a_0 is the Bohr radius. The constants .8 and 1.2 are fitting parameters from Barrett's simulation, d = d(Å) is the axial atomic spacing and E = E(MeV) is the energy of the incident ion beam. F_{RS} is proportional to the square root of the continuum potential and is tabulated in other sources.[1,19] There is an uncertainty in the half angle of 5-10% associated with the plane in which the tilt scan is performed. The one dimensional rms thermal vibration amplitude is shown below

$$u_1 = 12.1 \left\{ \left(\frac{\phi(x)}{x} + \frac{1}{4} \right) \frac{1}{M2\ \theta_D} \right\} \text{Å} \qquad 4.2.2$$

Where $\phi(x)$ is the Debye function $\frac{1}{x}\int_0^x \frac{dt\,t}{e^t - 1}$ and x equals θ_D/T, θ_D the Debye temperature and T the sample temperature are in degrees Kelvin; M2 is in atomic mass units.

The minimum yield is given by the following equation

$$\chi_{min} = 18.8\ N\ d\ u_1^2 (1 + \xi^{-2})^{1/2} \qquad 4.2.3$$

$N\ d\ u_1^2 \pi$ represents the fractional area in the transverse plane occupied by thermally vibrating surface atoms. ξ is equal to $126\ u_1\ / \psi_{1/2}\ d$. N is the atom density per unit cell. χ_{min} thus has a weak dependence on energy through ξ along with a stronger dependence on temperature through u_1 . This equation represents what would be expected for a minimum yield determined just behind the surface peak for a depth of 1000 Å.

Surface peak yield can be estimated through

$$L = (1 + \xi^2)^{1/2} \qquad 4.2.4$$

L is the number of atoms per string contributing to the suface peak yield. The factor 1 is the surface atoms' contribution, necessarily energy and temperature independent. The term ξ^2 is the contribution from partially shadowed atoms in the first few monolayers of the crystal. L increases with both increasing temperature (through u_1) and energy (inversely through $\psi_{1/2}$).

The number of atomic monolayers contributing to the experimental surface peak yield can be determined through the following equation

$$L' = \frac{A}{H} \frac{dE}{[\ S\ ]} \frac{1}{d_{\langle\rangle}} \qquad 4.2.5$$

The total number of displaced atoms being equal to L'- L. A is the area of the surface peak yield in counts. H is the height of the random spectra at the surface, dE is the energy width of a channel in the multi-channel analyser, [S], defined in equation 3.2.5, is the stopping power factor and $d_{<>}$ is the axial lattice constant. These are illustrated in figure 4.3.

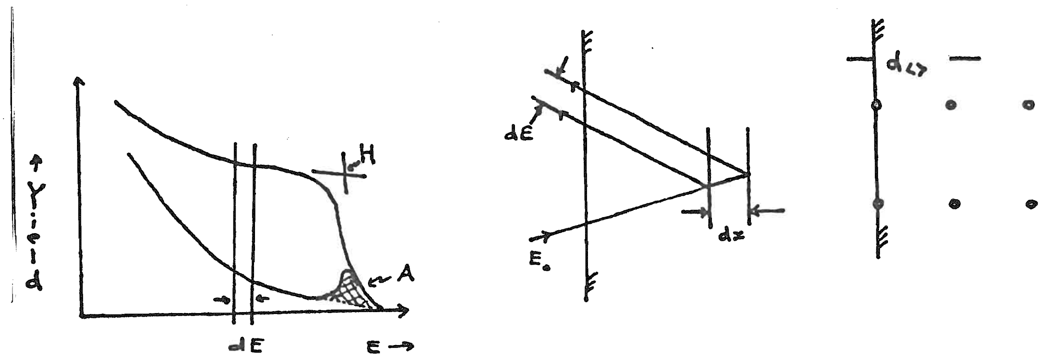

figure 4.3: illustrations of parameters in equation 4.2.5

In the surface approximation with $\theta_1 = \theta_2 = 0$ for the Guelph data equation 3.2.5 can be written as

$$[\ S\ ] = (k^2 + 1)\ S(E_o) \qquad 4.2.6$$

Where the kinematic factor, k^2, is given by equation 3. .1.

The following table is a result of an evaluation of experimental data gathered at Guelph using the equations just presented. These measurements were made at room temperature though there may have been some radiative heat loss due to the fact that the cryo-shield was in close proximity and was being held at liquid nitrogen temperatures. The Debye temperature has been taken as 315K and rms thermal vibration amplitudes are tabulated in Appendix I.

Table 4.1: Guelph University Data

1 MeV H+						
Minmum Yield		sample	axis	χ min	+/-	comments
	exp.	pure	⟨110⟩	.027	12%	polished
	"	.01% In	⟨110⟩	.025	12%	"
	theor.		⟨110⟩	.025	20-30%	
Axial Half Angle		sample	axis	ψ 1/2	+/-	comments
	exp.	.01%In	⟨110⟩	0.72	.08	polished
	theor.		⟨110⟩	0.78	.06	"
1 MeV He+						
Minmum Yield		sample	axis	χ min	+/-	comments
	exp.	pure	⟨110⟩	.025	18%	polished
	"	.01%In	⟨110⟩	.028	18%	"
	theor.		⟨110⟩	.025	20-30%	
Axial Half Angle		sample	axis	ψ 1/2	+/-	comments
	exp.	.01%In	⟨110⟩	1.0	.04	polished
	theor.		⟨110⟩	1.1	.08	
Surface Disorder ⟨110⟩ axis		sample	atoms/string	+/-		comments
	exp.	pure	3.6	35%		polished
		.01%In	3.6	35%		"
	theor.		4.0	14%		surface + thermal

A further test of the preparation technique can be made from an examination of dechanneling data for several crystals,figure 4.4.

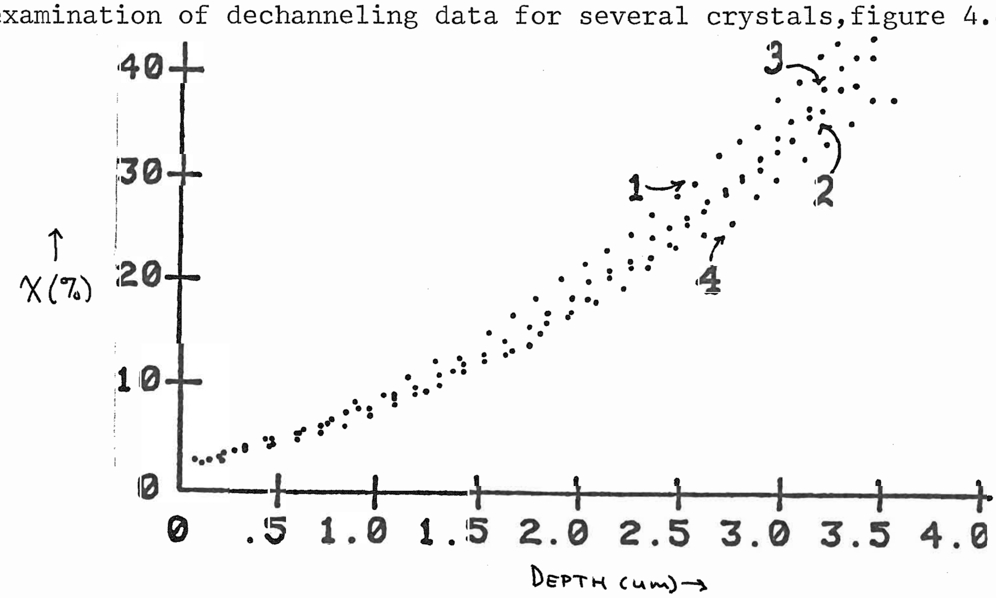

figure 4.4: Dechanneling fractions for several copper crystals for 1 MeV protons along the ⟨110⟩

Curves 1 and 2 are from slices of the same crystal, curve 2 has been taken after annealing. Curve 3 and 4 were runs from each machine and are from a slice of a totally different crystal.

4.3 Discussion

Annealing and X-ray data indicate that the bulk of each crystal is well ordered and that if there are any defects they are probably immobile.

Agreement between observed minimum yields and axial half angles and results of the computer simulation for a perfect crystal is good and would tend to support the contention that the surface is well ordered. Since agreement between theory and experiment is good for the minimum yields it is therefore probable that the uncertainty in choosing a Debye temperature is not as serious as the error analysis value of 20-30% would tend to indicate; thus the theoretical accuracy is likely much better than that recorded.

Surface peak yields indicate that the lattice is well ordered out to the surface, though patches of disorder may exist. Lower experimental values are most likely due to radiative cooling; no monitor of the target temperature could be made and it was therefore assumed to be at room temperature.

Dechanneled fraction curves are the same within their experimental accuracy and they would tend to indicate again that the crystals are highly ordered. Since annealing had no visible effect it can also be concluded that no significant concentration of mobile defects exist in the crystals.

Mozaic spread was found to be less than 1/2 of a degree when aligning the beam along the ⟨110⟩ axis over the surface of the crystal. The beam angular divergence was less than .06 of a degree.

Hence, in conclusion, the techniques used in handling and preparing crystals has not injured their integrity and thus the experimental data will be that of a well ordered crystal with undeformed channels extending to the surface.

5. Results and Discussion: Introduction

In this chapter descriptions, physical interpretations and theoretical predictions will be made for experimental data from Chalk River. Experimental and theoretical results, some of which are tabulated in appendix II, are presented in graphical form. The Debye temperature has been taken to be 315K.

5.1 1 MeV H+ on Copper

The following tilt scans were taken within an energy/depth window, just behind the surface peak, of width 13 channels from channel 186 to 198; this is equal to approximately 0.3 microns. The surface edge is at channel 202 and channel widths are approximately 4.7 keV / channel.

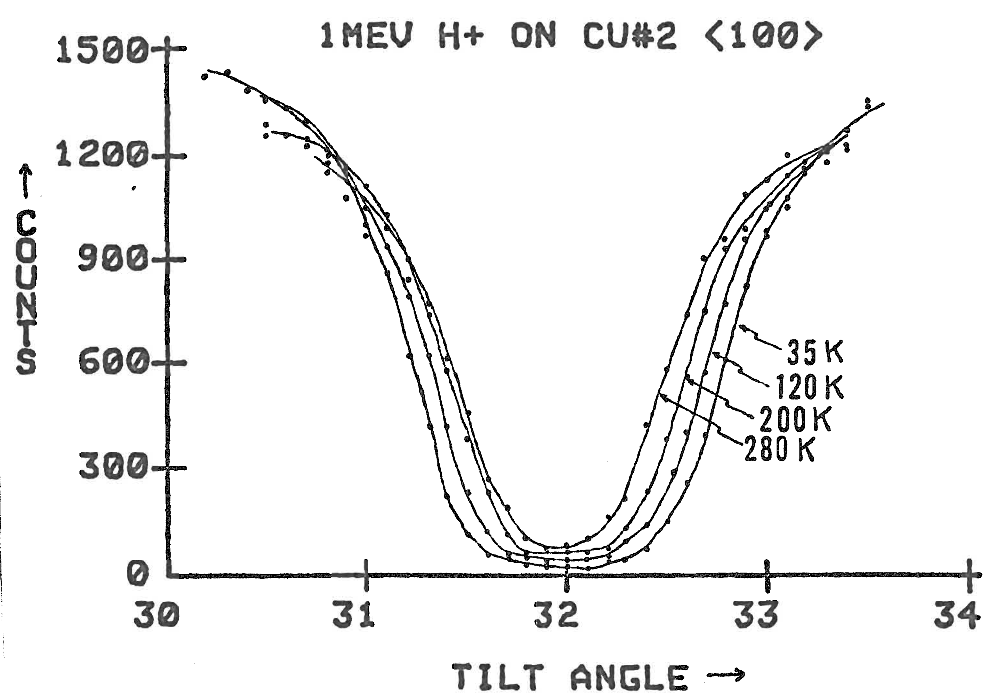

figure 5.1: temperature dependent tilt scans

Tilt scans in figure 5.1 show the dependence of nuclear back scattering yield on tilt angle and thermal vibration amplitude; as vibration amplitude increases with temperature the dip and axial half angle decrease. Increase in thermal vibration amplitude will result in spreading of the continuum string and thus; its ability to steer ions away from the string decreases (this can be attributed to changes in the string potential). Also, the fact that string atoms move closer to the channel centre results in an increase in the probability of lower transverse energy ions undergoing large angle nuclear scattering and therefore contributing to the backscattered yield. Thus the increase in backscattered yield at lower energies will result in a decrease in the axial half angle.

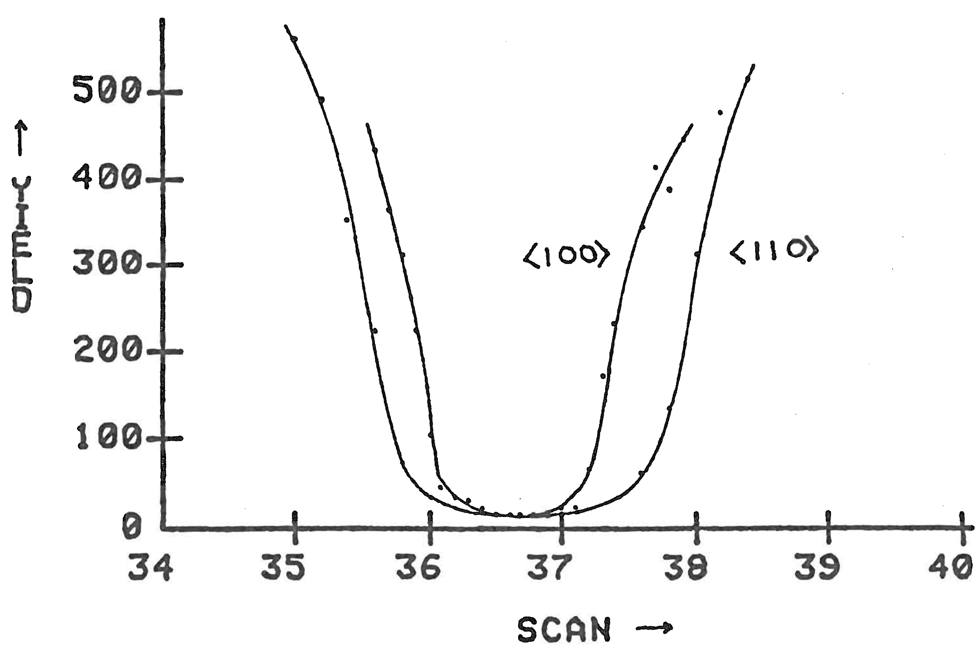

figure 5.2: axial dependent tilt scans

Tilt scans in figure 5.2 show the yields' dependence on channel geometry as a result of the different axial lattice parameters. Along the ⟨100⟩ axis the axial parameter is larger than for the ⟨110⟩ axis. This results in a decrease in the critical angle and, see equation 4.2.1, therefore a decrease in the axial half angle. This can be understood in the context that increasing the spacing between string atoms will decrease their ability to steer ions away at lower transverse energies and thus an increase in backscattered yield would be expected.

As a consequence of the statistical nature of the backscattered yield the data has a precision given by the square root of the yield divided by the yield. Thus the error in $\psi_{1/2}$ is approximately 10%. Experimental and theoretical axial half angles are tabulated in table 5.1

table 5.1: Axial Half Angles

		35K	120K	200K	280K	
⟨100⟩ 1.0 MeV						
	theoretical	0.81	0.74	0.69	0.65	(7%)
	experimental	0.78	0.69	0.62	0.56	(10%)
⟨110⟩ 1.0 MeV						
	theoretical	0.96	0.88	0.82	0.80	(7%)
	experimental	0.98	0.88	0.76	0.70	(10%)

From table 5.1 a comparison between experimental and theoretical axial half angles shows good agreement. This indicates that the quality of the crystal appears to be good within the first one thousand atomic layers. A preliminary beam alignment was always performed on the periphery of the crystal just prior to this final alignment.

Before aligned spectra were recorded it was necessary to take quick tilt and azimuthal scans through the axis in order to verify the beam/axis alignment. The angle choosen from each scan was the average of the mid-points from either side of the tilt scan yield through the dip. Reproducibility was very good and the precision was about one hundredth of a degree.

In figure 5.3 a tilt scan down an axis with two windows set at different depths was recorded. Alignment of the tilt scan yields tends to indicate that the channel is undeformed. Increasing yield with depth at a specific tilt angle is partially a consequence of the increase in scattering cross section with decrease in energy and, also, the increase in average transverse energy of the channeled fraction.

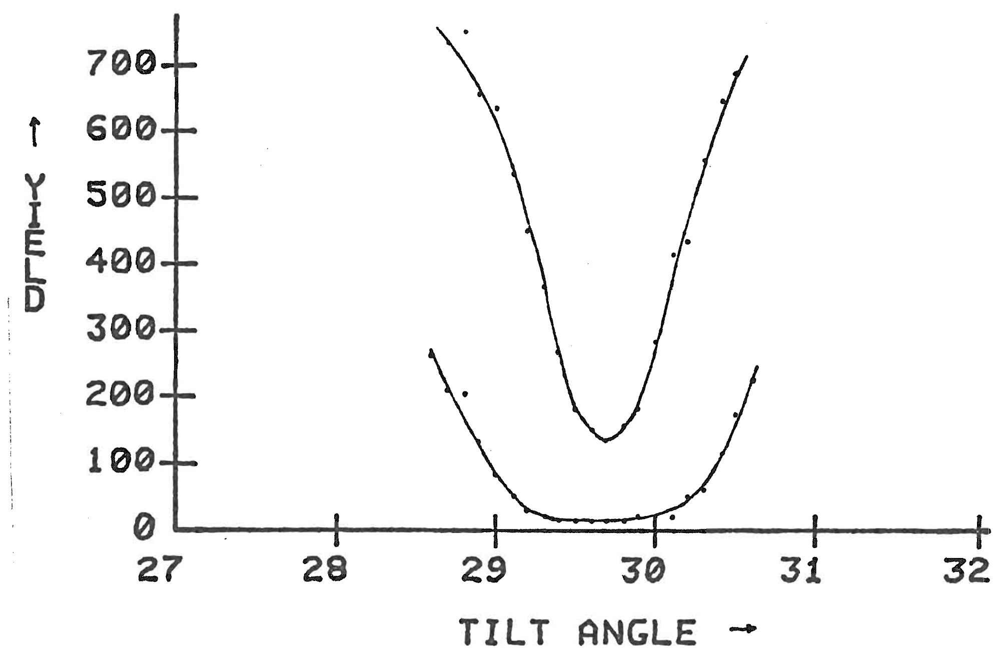

figure 5.3: tilt scans at different depths

Figures 5.4 and 5.5 represent the temperature and axial dependence of the RBS backscattered yields. From these spectra dechanneled fractions shall be extracted.

RBS yields have been plotted against channel number. Decreasing channel number is equivalent to increasing depth and decreasing energy though these relationships are nonlinear.

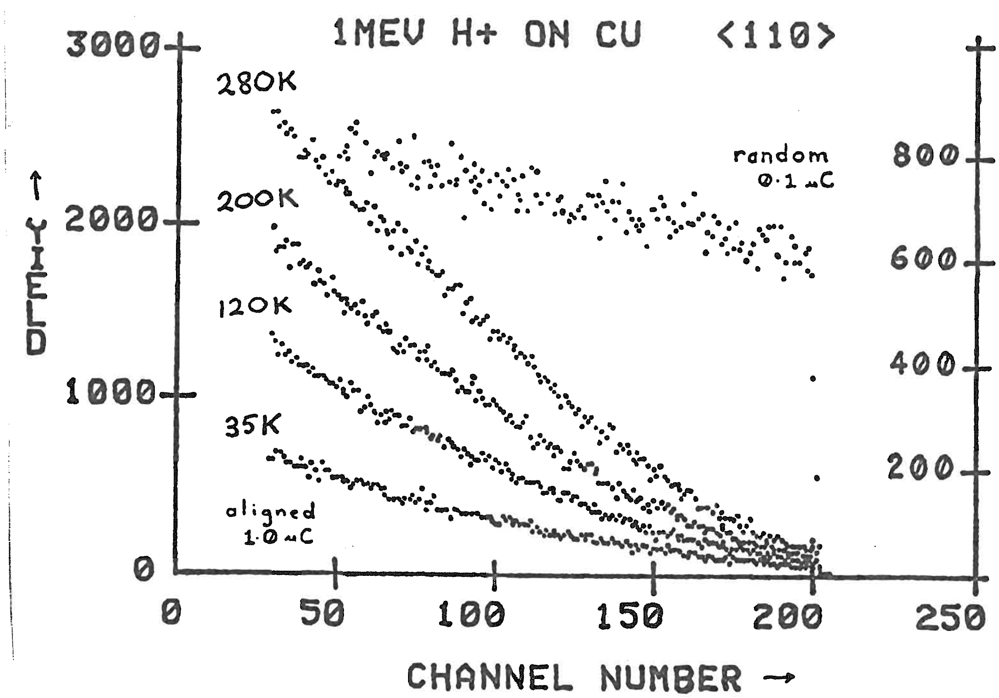

figure 5.4: temperature dependent RBS spectra

Figure 5.4 shows a typical group of RBS spectra for 1MeV protons on copper along the ⟨110⟩ axis. A strong dependence of the aligned yield with increasing temperature is observable. This dependence is a result of the increase in thermal displacement of lattice atoms with increasing temperature and results in an increase in force fluctuation experienced by channeled ions. This increases the probability of transition to higher transverse energies at shallower depths and thus to the dechanneled fraction. Larger fractions of ions in the dechanneled portion of the beam will result in an increase in backscatter yield.

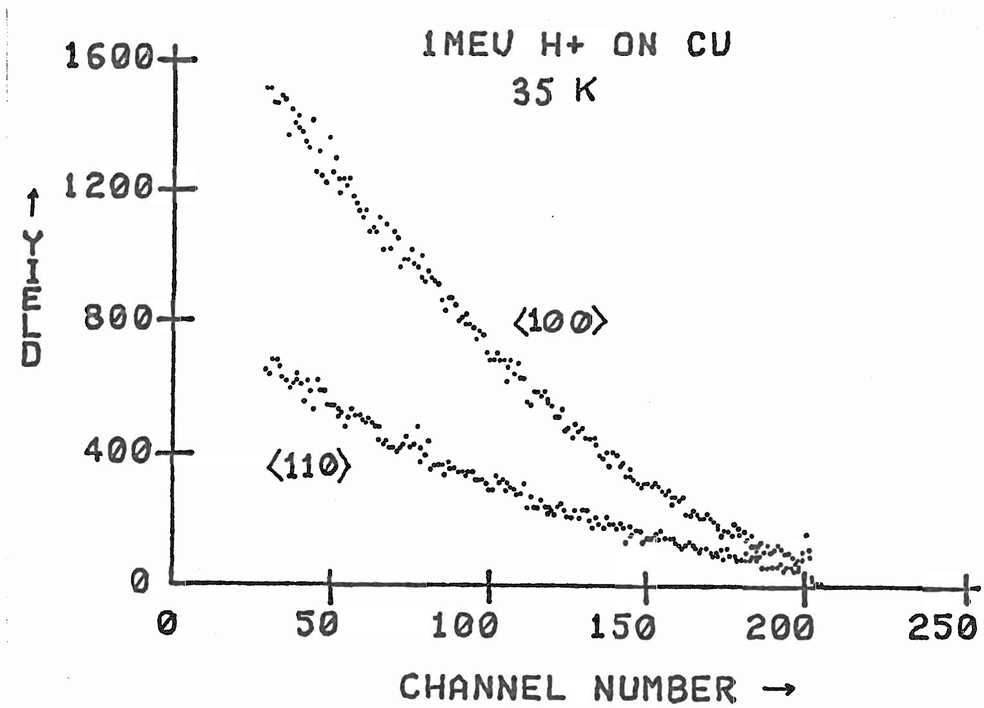

figure 5.5: axial dependent RBS spectra

Another observable feature from RBS spectra is the axial dependence of aligned yield, figure 5.5. The controlling factors are the same as those discussed for the tilt scans.

χ_{min} values in table 5.2 were extracted from RBS spectra by averaging yields over 5 channels just behind the surface peak for both the aligned and random spectra and then taking their ratio. Five channels corresponds to a depth of approximately 0.1 um.

table 5.2: Chi Minimum

		35K	120K	200K	280K	
⟨100⟩ 1.0 MeV						
	theoretical	0.013	0.020	0.030	0.040	(20-30%)
	experimental	0.015	0.021	0.033	0.044	(12%)
⟨110⟩ 1.0 MeV						
	theoretical	0.009	0.014	0.021	0.028	(20-30%)
	experimental	0.009	0.014	0.020	0.027	(12%)

From table 5.2 a comparison between experimental and theoretical values, using a Debye temperature of 315 K, shows very good agreement (discussion of experimental error in chapter 4). This parameter will be discussed a little later on in the text of this section.

Figures 5.4 and 5.5 are representative spectra plotted from the data in appendix II. We proceed with a discussion based on Moore's[13] method of analysis of experimental data and Matsunami and Howe's[11] theoretical treatment. Curves are distinguished by dots for experimental values and solid lines for theoretical values.

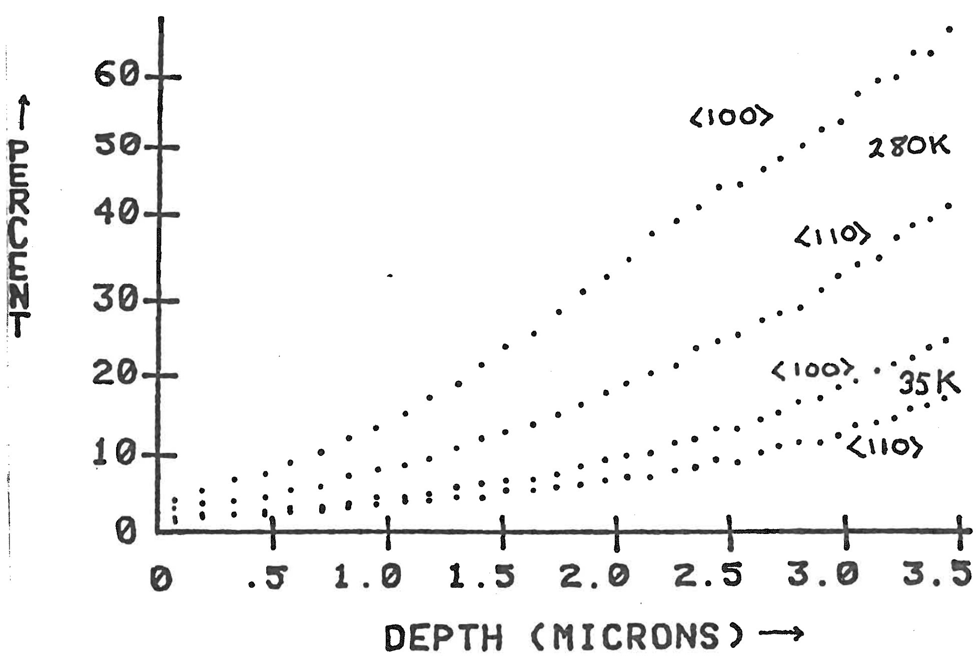

figure 5.6: axial dependent dechanneled fractions, 280K

Large differences in dechanneled fractions for the two axes at the same temperature is easily observed in figure 5.6. A good theoretical description should yield a good fit at all temperatures. Variation in the rate of change of dechanneling for shallow and large depths will be demanding upon the theoretical treatment.

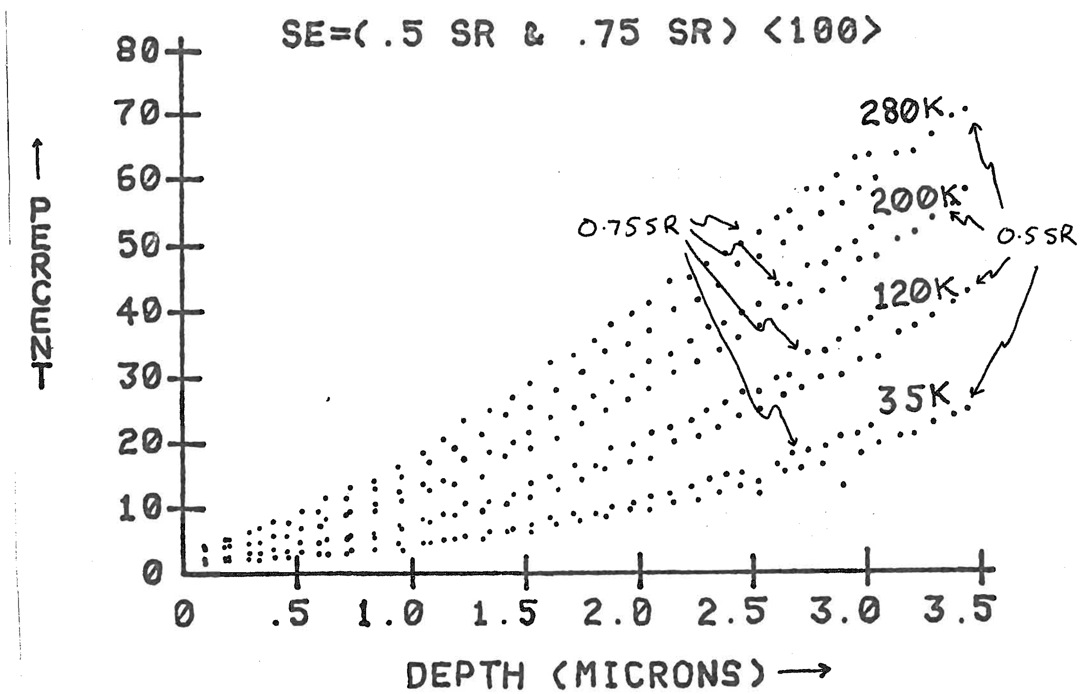

figure 5.7: channel stopping power dependent dechanneled fractions, <100>

Figure 5.7 shows the sensitivity of dechanneled fractions on channel stopping power choosen for the analysis of experimental data. It is customary to use a value equal to 0.5 times the random stopping power. This corresponds to the stopping power which would be expected for well channeled ions. For the channeled beam as a whole, the average channel stopping power would be expected to be greater than this minimum value. One can get a feeling for the average stopping power from data generated from the theoretical model of Matsunami and Howe,appendixII. Figure 5.7 shows the effect of varying this parameter on the dechanneled fraction. The obvious result that particles will penetrate to greater depths for lower stopping powers is evident.

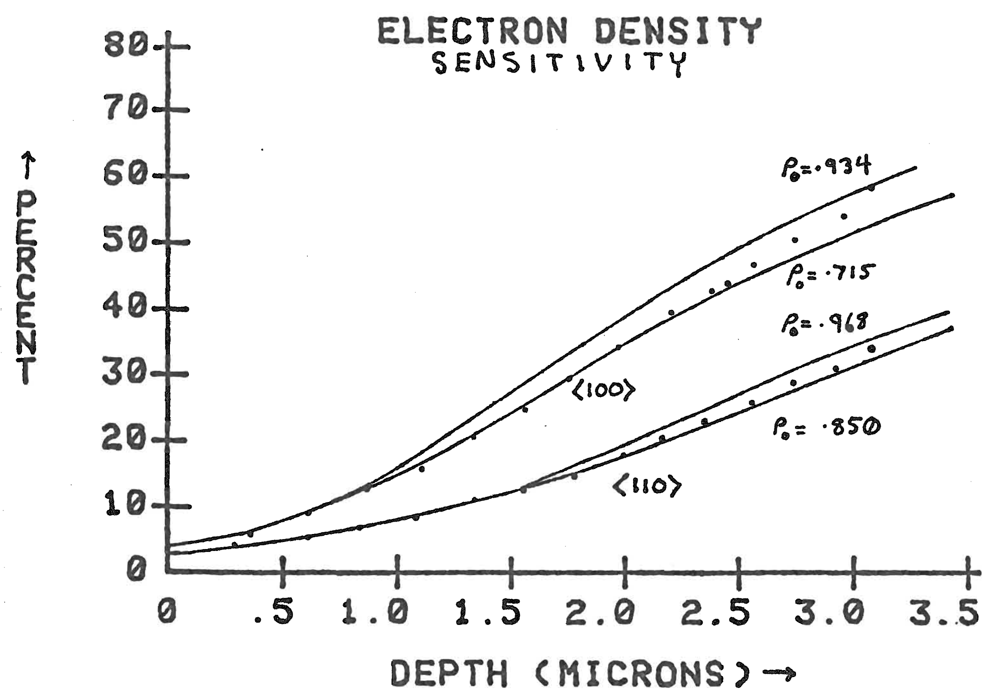

figure 5.8: electron density dependent theoretical dechanneled fractions

Figure 5.8 shows the sensitivity of the theoretical dechanneled fractions as a result of varying the constant electron density parameter for the channel centre. Nuclear scattering dominates dechanneling at shallow depths. The effect of varying electron density is to wag the dechanneled fraction at greater depths; this results since it takes time for electronic collisions to raise the average transverse energy of well channeled ions to the point where nuclear scattering becomes significant.

Through adjustment of the constant electron density parameter in the channel centre the theoretical dechanneling curves which result in a best fit of the experimental data along the ⟨110⟩ axis is 0.875 $Å^{-3}$ and for the ⟨100⟩ axis it is 0.7325 $Å^{-3}$.

Figures 5.9 and 5.10 show experimental and theoretical dechanneled fraction curves from an analysis of the experimental data using a channel stopping power of 0.5 times the random value and the best fit electron densities. Comments on these graphs will be made after figure 5.10.

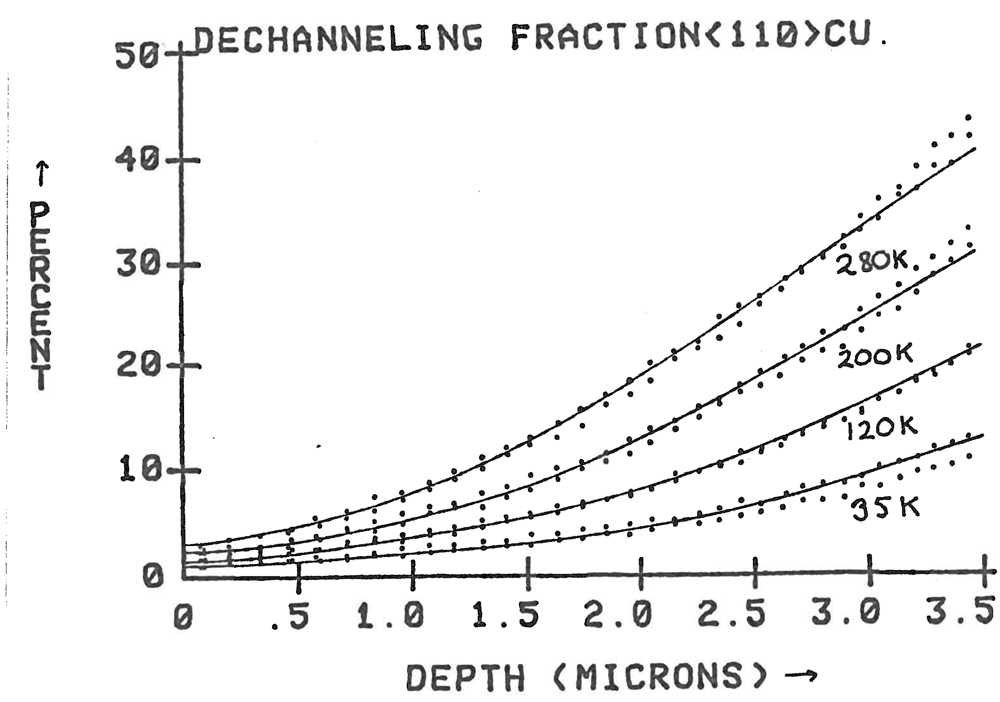

figure 5.9: temperature dependent dechanneled fractions, ⟨110⟩

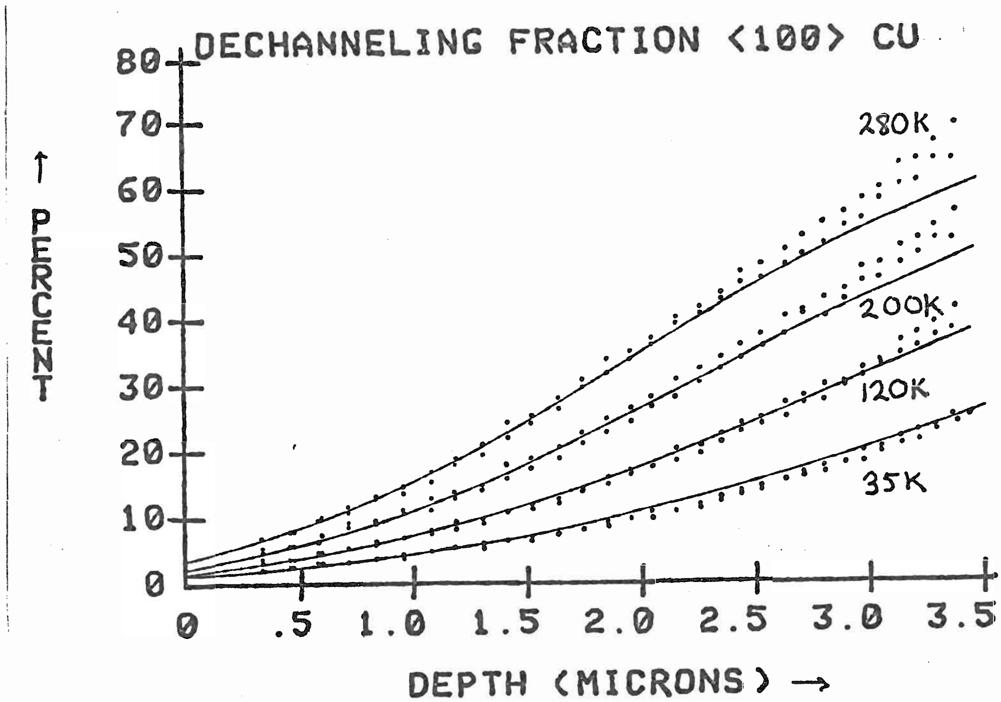

figure 5.10: temperature dependent dechanneled fractions, ⟨100⟩

Before description of the figures a table of values showing the range of variation of dechanneling fractions with temperature and depth will be shown.

table 5.3: Range of variation in dχ/dz with z , T from figures 5.9 and 5.10

	⟨110⟩ 0.5 um		⟨110⟩ 2.5 um		curve	⟨100⟩ 0.5 um		⟨100⟩ 2.5 um	
	%	%/um	%	%/um		%	%/um	%	%/um
280 K	4.5	4.6	26	14	(4)	9	12	45	18
200 K	3.0	3.2	18	11	(3)	6	9	35	18
120 K	2.3	2.4	12	8	(2)	4	6	24	13
35 K	1.8	1.4	6	5	(1)	2	3	15	9

Figures 5.9 and 5.10 result from an analysis of the spectra of 1MeV protons on copper for the ⟨100⟩ and ⟨110⟩ axes. It is apparent that theoretical and experimental curves match extremely well. Deviations only occur at large depths and these increase slightly with increasing temperature. The tailing off of the theoretical values to values lower than the experimental values appears to be occurring above 20 to 30% dechanneling.

In table 5.3 slopes change by up to factors of 4,3 and 2 as functions of temperature, depth and axis respectively. The theoretical treatment yields results comparable to the experimental results over a wide range of values. The ability of the theoretical description to match the large changes in dechanneled fractions and their rates of change for quite different geometries as functions of both depth and temperature is a testament to the treatment of the physical processes.

Defect dechanneling appears to be insignificant for several reasons. First, surface parameters indicate well ordered crystals with undeformed channels, at least in the surface region. Second, yields for two different crystals, having different histories, match very well and is thus self corroborating. Lastly, variation of dechanneled fractions with z and T in accordance with theory lends to the argument that crystal quality is good. Thus dechanneling due to residual defects appears to be insignificant. Also, since the crystals appear to be of high quality then χ_{min} values are probably also good.

Therefore the poor precision in the theoretical χ_{min} values is probably exaggerated.

One aspect investigated was the possibility that defects might have been induced during the course of the experiment.

While exposing crystals to the ion beam spectra were recorded with increasing temperature in order that the majority of well channeled ions would reach their maximum depth and would thus have a less detrimental effect upon later dechanneled fractions. Also, it is expected that damage introduced through implanting of protons will probably be annealed out at the temperatures of the investigation. When the temperature was cycled back to the starting temperature after a day of channeling no evidence of induced damage could be identified from the RBS spectra.

5.2 2 MeV H+

For the 2 MeV spectra the surface edge is at channel 202, alignment of the crystal was performed with a window 28 channels wide from channel 167 to 194 and which is equal to approximately 2.0 microns. The channel width was approximately 9.4 keV / channel. χ_{min} were calculated using data averaged over 3 channels (equivalent to about 0.2 microns) just behind the surface peak.

table 5.4: Chi Minimum

		56K	170K	280K	
⟨100⟩ 2.0 MeV					
	theoretical	0.013	0.025	0.039	(20-30%)
	experimental	0.018	0.036	0.058	(12%)
⟨110⟩ 2.0 MeV					
	theoretical	0.009	0.018	0.028	(20-30%)
	experimental	0.009	0.018	0.031	(12%)

The data in table 5.4 indicates that even though the ⟨110⟩ axis appears to be alright the ⟨100⟩ axis is probably marginal at best. When viewed in the light of the probable increased precision of the theoretical data then the data presented here indicates that the crystal quality is poor and thus it can not be compared directly with Matsunami and Howe's theoretical dechanneling curves.

Using the same electron density for the channel centre determined for a best fit of the 1 MeV data above, theoretical dechanneling curves were generated for 2MeV protons on copper for the ⟨100⟩ and ⟨110⟩ axes. Plots of these against experimental data are shown in figure 5.11 and 5.12.

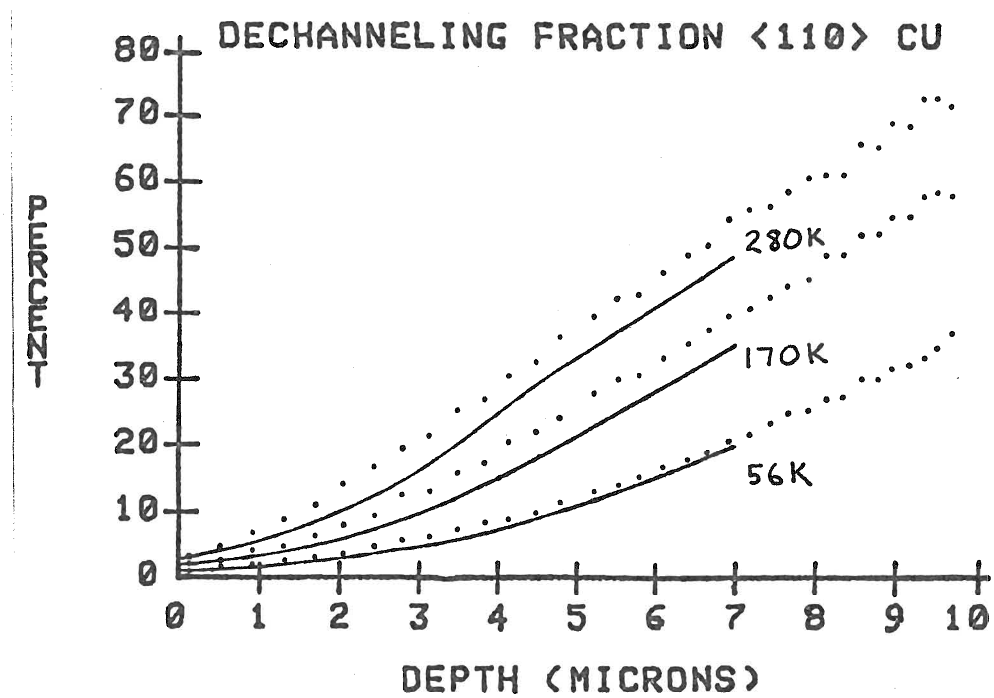

figure 5.11: temperature dependent dechanneled fractions, ⟨110⟩

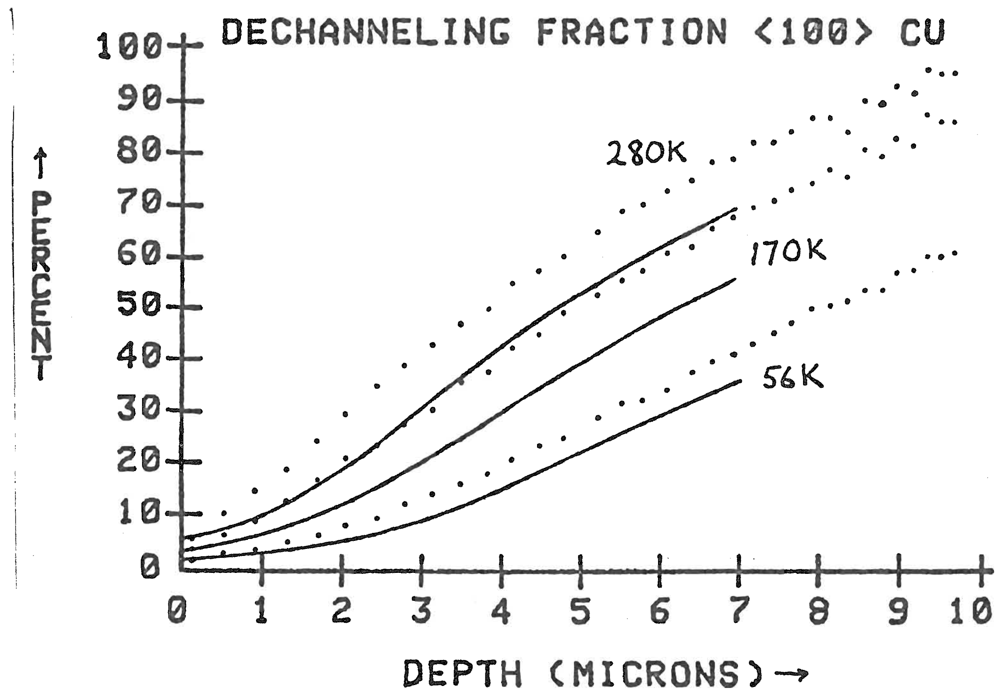

figure 5.12: temperature dependent dechanneled fractions, ⟨100⟩

The fit for these sets of data are relatively poor, 25% at shallow depths decreasing to 10% at larger depths. The low temperature fits are fair and the fits get worse with increasing temperature.

One mistake, in hindsight, may be that angular scans were not taken over a small enough energy range. Thus the half angles could not be used as a measure of the quality of the crystal.

The fits along with the minimum yields appear to indicate that the crystal is flawed in some way, most probably in the first two microns as attested by the quick divergence of the experimental and theoretical values for the ⟨100⟩ axis, either through the prevacuum preparation technique or some inherent or induced flaw such as a high defect concentration.

Unfortunately a second run on a different crystal was not performed as a check on the validity of the first run. Lack of data on the other suface parameters hampers any attemp to make a definative statement about crystal quality other than that it is dubious.

5.3 A Look at Electron Densities

Equipotential plots in reduced energy for the ⟨100⟩ and ⟨110⟩ axes are shown in figure 5.13 along with cross sections through electron density distributions shown in figure 5.14; radii are indicated by letters in figure 5.13. These were produced using the standard potential; if a Moliere potential were used then electron densities at the channel centres would be about twice the values shown and thus correspond more closely with constant electron densities from the fitting procedure.

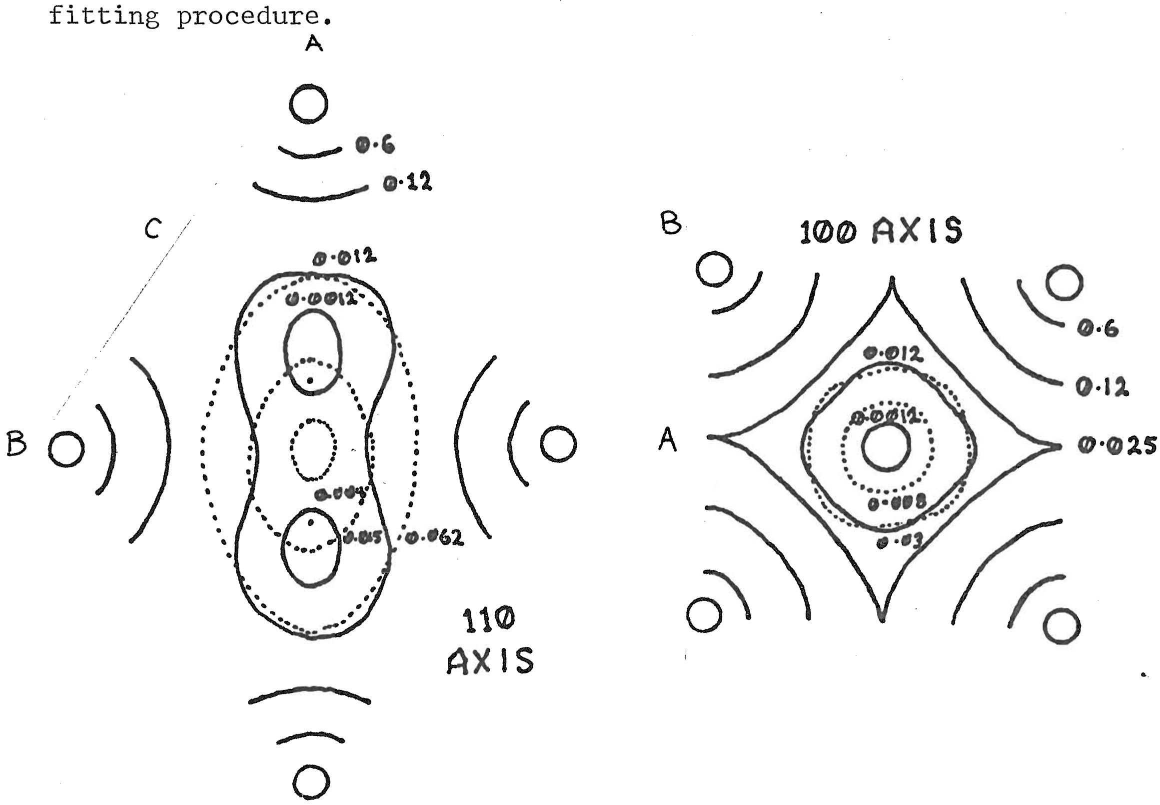

figure 5.13: Equipotential plots in reduced energy for the ⟨100⟩ and ⟨110⟩ axes

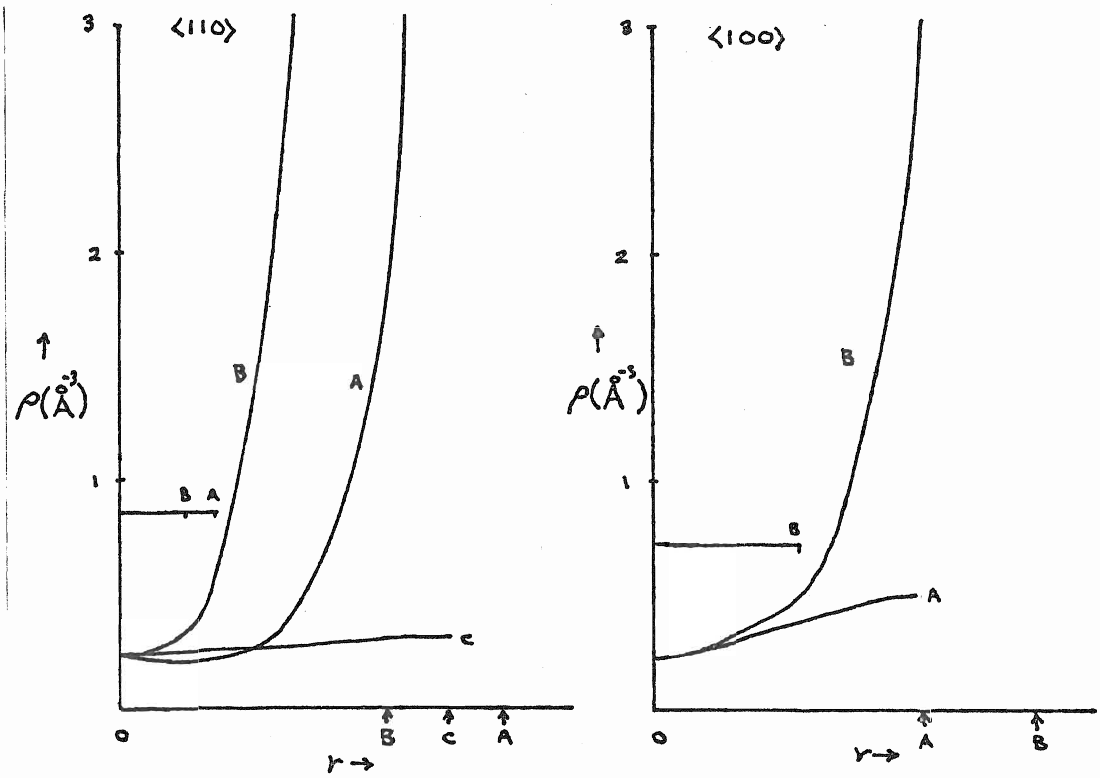

figure 5.14: Electron density cross sections for the ⟨100⟩ and ⟨110⟩ axes

Another measure of the validity of the constant electron densities used can be seen when the outer 11 electrons in the 3d and 4s shells are averaged over the atomic volume. Cooresponding to this calculation the electron density is slightly more than 0.9 electrons per cubic angstrom.

Continuity is observed between channel centre and string regions for both equipotential and electron density plots for the ⟨100⟩ axis; the agreement with the ⟨110⟩ axis is less readily justified due to the large discontinuity of the electron density with the long axis. The dotted potential lines in figure 5.13 were calculated assuming the constant electron densities from the fitting procedure. Thus, at least for the more symmetric axis, using the electron density as a fitting parameter seems justified.

5.4 Summary

In summary, theoretical and experimental dechanneling fraction curves match excellantly for 1MeV protons on copper when using constant channel centre electron densities of 0.875 $Å^{-3}$ and 0.7325 $Å^{-3}$ for the ⟨110⟩ and ⟨100⟩ axes respectively. Electron densities and their respective interatomic potentials were compared to those expected from a Moliere approximation and the 0.9 electrons per cubic angstrom electron density expected when the outer 3d and 4s electrons are averaged over their atomic volume. The relatively good agreement indicates that the electron densities obtained from the fitting procedure are reasonable. Subsequently one may conclude that for good quality single crystals both the experimental and theoretical analyses are well founded and thus the continuum string approach which yields excellant results with respect to channeling phenomena has shown itself to be very useful in modeling dechanneling phenomena.

Surface parameters have been shown to be useful in determining the quality of single crystals, namely in the case of the 2MeV data. The conclusion which may be drawn from the minimum yields along with the poor match with the theoretical predictions is that the crystal was either damaged or that defects were encountered while polishing the crystal. This experience also highlights the necessity of taking spectra with several good crystals in order to have some confidence in the results.

References

References

1.. Gemmell, D.S.; Rev. Mod. Phys. 46 129 (1974).

2.. Dearnley, G., Freeman, J.H., Nelson, R.S., Stephen, J.; Ion Implantation (North-Holland, 1973).

3.. Morgan, D.V., Channeling (Wiley,1973).

4.. Townsend, P.D., Kelly, J.C., Hartley, N.E.W.; Ion Implantation, Sputtering and their Applications (Academic Press, 1976).

5.. Chu, W.K., Mayer, J.W., Nicolet, M.A.; Backscattering Spectrometry (Academic Press, 1978).

6.. L'Ecuyer, J., Davies, J.A., Matsunami, N.; Nucl. Instr. Meth. 160 337 (1979).

7.. Lindhard, J.; K. Dan Vidensk. Selsk. Mat. Fys. Medd. 34, Nr. 14 (1965).

8.. Bonderup, E.H., Esbensen, H., Andersen, J.U., Shiott, H.E.; Rad. Eff. 12 261 (1972).

9.. Shiott, H.E., Bonderup, E., Andersen, J.U., Esbensen, H.; Atomic Collisions in Solids Vol.2, 843 (Plenum, N.Y., 1975).

10. Pederson, M.J., Andersen, J.U., Elliott, D.J., Laesgaard, E.; Atomic Collisions in Solids Vol.2, 863 (Plenum, N.Y., 1975).

11. Matsunami, N. and Howe, L.M.; Rad. Eff. 51 111 (1980).

12. Kitagawa, M. and Ohtsuki, Y.H.; Phys. Rev.B 8 3117 (1973).

13. Moore, J.A.; Nucl. Instr. Meth. 174 577 (1980).

14. Howe, L.M., Moore, J.A., Matsunami, N. and Wright, D.R.; Rad. Eff. 70 197 (1983).

15. Lindhard, J.; K. Dan Vidensk. Selsk. Mat. Fys. Medd. 28, Nr. 8 (1954).

16. Anderson, H.H. and Ziegler, J.F.; Hydrogen Stopping Powers and Ranges in all Elements vol 3 (Pergamon, 1977).

17. Ziegler, J.F.; Helium Stopping Powers and Ranges in all Elements vol 4 (Pergamon, 1977).

18. Barrett, J.H.; Phys. Rev. B 3 1527 (1971).

19. Appleton, B.R. and Foti, G.; Ion Beam Handbook for Material Analysis, J.W. Mayer & E. Rimini (Academic Press, NY,1977), ch.3.

20. Kittel, C.; Introduction to Solid State Physics (John Wiley, N.Y., 1976).

Appendic es

The theoretical calculation requires several inputs which are listed in the following table.

energy (MeV)	axis	temperature (K)	electron density ($Å^{-3}$)	displacement rms (Å)	mid string potential	nuclear correction factor
1.0	⟨110⟩	35	0.8750	0.06270	0.02913	0.340919
		120		0.08083		
		200		0.09869		
		280		0.11563		
1.0	⟨100⟩	35	0.7325	0.06270	0.06215	0.312463
		120		0.08083		
		200		0.09869		
		280		0.11563		
2.0	⟨110⟩	56	0.8750	0.06619	0.02913	0.357188
		170		0.09259		
		280		0.11563		0.357176
2.0	⟨100⟩	56	0.7325	0.06619	0.06215	0.331640
		170		0.09259		
		280		0.11563		0.331628

Theoretical dechanneling and electronic stopping power values for channeled 1.0 MeV protons in pure copper, ⟨110⟩.

depth	35K		120K		200K		280K	
(um)	chi	Se	chi	Se	chi	Se	chi	Se
0.00	.0052	.8364	.0074	.8363	.0091	.8361	.0116	.8360
0.05	.0058	.8390	.0084	.8389	.0106	.8387	.0138	.8386
0.10	.0064	.8414	.0094	.8412	.0122	.8411	.0160	.8409
0.15	.0070	.8435	.0104	.8433	.0137	.8432	.0182	.8431
0.20	.0076	.8455	.0113	.8453	.0152	.8451	.0203	.8450
0.25	.0081	.8473	.0123	.8471	.0166	.8469	.0224	.8469
0.30	.0087	.8491	.0133	.8488	.0181	.8486	.0245	.8486
0.35	.0093	.8508	.0142	.8504	.0195	.8502	.0265	.8502
0.40	.0099	.8524	.0152	.8520	.0210	.8517	.0286	.8517
0.45	.0105	.8539	.0161	.8543	.0224	.8532	.0307	.8531
0.50	.0110	.8553	.0171	.8548	.0239	.8545	.0329	.8544
0.55	.0116	.8567	.0181	.8562	.0254	.8558	.0351	.8557
0.60	.0122	.8581	.0191	.8574	.0269	.8571	.0374	.8569
0.65	.0128	.8594	.0201	.8587	.0285	.8583	.0398	.8581
0.70	.0135	.8606	.0211	.8598	.0302	.8594	.0424	.8592
0.75	.0141	.8618	.0222	.8609	.0319	.8605	.0450	.8603
0.80	.0147	.8629	.0233	.8620	.0337	.8615	.0478	.8612
0.85	.0154	.8640	.0245	.8630	.0356	.8625	.0508	.8622
0.90	.0161	.8651	.0257	.8640	.0376	.8634	.0539	.8630
0.95	.0168	.8661	.0270	.8650	.0397	.8643	.0572	.8639
1.00	.0175	.8671	.0283	.8659	.0419	.8652	.0607	.8646
1.10	.0190	.8690	.0311	.8675	.0467	.8667	.0683	.8659
1.20	.0207	.8707	.0343	.8690	.0520	.8680	.0767	.8670
1.30	.0225	.8723	.0378	.8704	.0579	.8691	.0859	.8678
1.40	.0245	.8737	.0416	.8715	.0644	.8699	.0958	.8682
1.50	.0266	.8751	.0459	.8725	.0715	.8706	.1066	.8683
1.60	.0290	.8763	.0505	.8733	.0793	.8709	.1180	.8681
1.70	.0317	.8773	.0556	.8739	.0876	.8710	.1300	.8674
1.80	.0346	.8782	.0612	.8742	.0964	.8707	.1427	.8664
1.90	.0377	.8790	.0672	.8744	.1058	.8702	.1558	.8649
2.00	.0412	.8796	.0735	.8743	.1156	.8693	.1693	.8630
2.10	.0449	.8800	.0803	.8740	.1259	.8680	.1831	.8605
2.20	.0489	.8803	.0875	.8734	.1366	.8664	.1973	.8577
2.30	.0532	.8803	.0951	.8725	.1476	.8644	.2116	.8543
2.40	.0578	.8802	.1030	.8713	.1589	.8621	.2261	.8504
2.50	.0627	.8799	.1112	.8699	.1705	.8593	.2407	.8459
2.60	.0678	.8794	.1197	.8681	.1823	.8561	.2554	.8410
2.70	.0732	.8787	.1285	.8661	.1942	.8525	.2700	.8355
2.80	.0789	.8778	.1376	.8637	.2063	.8484	.2847	.8294
2.90	.0848	.8766	.1468	.8610	.2185	.8439	.2992	.8227
3.00	.0909	.8752	.1562	.8579	.2308	.8390	.3137	.8155
3.10	.0973	.8736	.1658	.8545	.2431	.8336	.3280	.8077
3.20	.1039	.8717	.1756	.8508	.2554	.8277	.3422	.7993
3.30	.1106	.8696	.1852	.8467	.2678	.8214	.3563	.7903
3.40	.1175	.8673	.1954	.8422	.2801	.8146	.3702	.7807
3.50	.1246	.8647	.2054	.8374	.2923	.8073	.3839	.7704
3.60	.1318	.8618	.2155	.8322	.3046	.7995	.3974	.7596
3.70	.1392	.8586	.2257	.8266	.3167	.7912	.4107	.7482
3.80	.1467	.8552	.2359	.8207	.3287	.7824	.4238	.7362
3.90	.1543	.8515	.2461	.8144	.3407	.7732	.4367	.7236
4.00	.1620	.8476	.2563	.8077	.3526	.7634	.4495	.7103

Theoretical dechanneling and electronic stopping power values for channeled 1.0 MeV protons in pure copper, ⟨100⟩.

depth	35K		120K		200K		280K	
(um)	chi	Se	chi	Se	chi	Se	chi	Se
0.00	.0075	.7423	.0107	.7420	.0130	.7416	.0166	.7413
0.05	.0086	.7464	.0126	.7462	.0162	.7460	.0212	.7459
0.10	.0098	.7501	.0146	.7500	.0193	.7499	.0257	.7500
0.15	.0110	.7535	.0166	.7535	.0223	.7535	.0300	.7538
0.20	.0122	.7568	.0185	.7568	.0252	.7569	.0342	.7573
0.25	.0133	.7600	.0204	.7599	.0281	.7600	.0384	.7606
0.30	.0145	.7630	.0223	.7629	.0310	.7630	.0426	.7637
0.35	.0157	.7659	.0243	.7657	.0340	.7659	.0469	.7666
0.40	.0168	.7687	.0262	.7685	.0370	.7687	.0514	.7694
0.45	.0180	.7714	.0282	.7711	.0401	.7713	.0561	.7721
0.50	.0192	.7741	.0303	.7736	.0434	.7739	.0610	.7746
0.55	.0205	.7766	.0324	.7760	.0468	.7763	.0662	.7771
0.60	.0218	.7790	.0346	.7784	.0504	.7786	.0717	.7794
0.65	.0231	.7813	.0370	.7806	.0541	.7808	.0775	.7815
0.70	.0245	.7836	.0394	.7827	.0581	.7828	.0836	.7836
0.75	.0259	.7857	.0420	.7847	.0623	.7848	.0901	.7854
0.80	.0274	.7878	.0447	.7866	.0668	.7866	.0970	.7872
0.85	.0289	.7897	.0476	.7884	.0715	.7884	.1042	.7888
0.90	.0306	.7916	.0506	.7902	.0765	.7900	.1117	.7902
0.95	.0323	.7934	.0538	.7918	.0817	.7914	.1196	.7915
1.00	.0341	.7951	.0572	.7933	.0873	.7928	.1278	.7926
1.10	.0380	.7983	.0645	.7960	.0991	.7950	.1450	.7942
1.20	.0424	.8012	.0726	.7982	.1119	.7967	.1633	.7951
1.30	.0472	.8037	.0814	.8000	.1256	.7977	.1824	.7951
1.40	.0525	.8058	.0910	.8013	.1402	.7981	.2022	.7944
1.50	.0583	.8076	.1013	.8021	.1555	.7979	.2224	.7928
1.60	.0646	.8090	.1123	.8024	.1713	.7970	.2430	.7904
1.70	.0715	.8100	.1239	.8021	.1877	.7954	.2637	.7871
1.80	.0788	.8107	.1360	.8014	.2045	.7931	.2845	.7829
1.90	.0866	.8109	.1486	.8000	.2215	.7901	.3052	.7779
2.00	.0949	.8107	.1616	.7981	.2388	.7864	.3258	.7719
2.10	.1036	.8101	.1749	.7956	.2561	.7819	.3461	.7651
2.20	.1127	.8090	.1886	.7926	.2735	.7768	.3661	.7573
2.30	.1221	.8076	.2024	.7890	.2908	.7709	.3858	.7487
2.40	.1319	.8057	.2164	.7849	.3081	.7642	.4051	.7391
2.50	.1420	.8034	.2306	.7801	.3252	.7570	.4240	.7287
2.60	.1523	.8006	.2448	.7748	.3422	.7489	.4424	.7173
2.70	.1628	.7974	.2591	.7689	.3589	.7401	.4603	.7051
2.80	.1736	.7938	.2734	.7625	.3754	.7306	.4778	.6920
2.90	.1844	.7897	.2876	.7554	.3917	.7203	.4949	.6780
3.00	.1955	.7852	.3018	.7478	.4077	.7094	.5115	.6631
3.10	.2066	.7803	.3159	.7397	.4234	.6977	.5276	.6474
3.20	.2178	.7749	.3299	.7309	.4388	.6853	.5433	.6308
3.30	.2291	.7691	.3438	.7216	.4539	.6722	.5586	.6134
3.40	.2405	.7629	.3575	.7117	.4688	.6584	.5735	.5952
3.50	.2518	.7562	.3712	.7013	.4833	.6439	.5880	.5763
3.60	.2632	.7491	.3846	.6903	.4976	.6287	.6020	.5565
3.70	.2746	.7416	.3979	.6788	.5116	.6129	.6158	.5361
3.80	.2860	.7336	.4111	.6667	.5253	.5964	.6291	.5149
3.90	.2973	.7253	.4240	.6541	.5387	.5793	.6422	.4930
4.00	.3086	.7165	.4369	.6409	.5519	.5615	.6549	.4704

Theoretical dechanneling and electronic stopping power values for channeled 2.0 MeV protons in pure copper, ⟨110⟩.

depth	56K		170K		280K	
(um)	chi	Se	chi	Se	chi	Se
0.00	.0055	.7409	.0087	.7406	.0116	.7441
0.05	.0058	.7431	.0095	.7428	.0128	.7463
0.10	.0062	.7452	.0102	.7449	.0141	.7484
0.15	.0065	.7472	.0110	.7469	.0154	.7504
0.20	.0069	.7490	.0117	.7487	.0166	.7523
0.25	.0073	.7508	.0125	.7505	.0178	.7541
0.30	.0076	.7524	.0132	.7522	.0190	.7558
0.35	.0080	.7541	.0139	.7538	.0202	.7575
0.40	.0084	.7556	.0146	.7554	.0214	.7591
0.45	.0087	.7572	.0153	.7569	.0226	.7607
0.50	.0091	.7586	.0161	.7583	.0238	.7622
0.55	.0094	.7601	.0168	.7597	.0250	.7637
0.60	.0098	.7615	.0175	.7611	.0261	.7651
0.65	.0102	.7628	.0182	.7624	.0273	.7665
0.70	.0105	.7642	.0189	.7637	.0286	.7679
0.75	.0109	.7655	.0197	.7649	.0298	.7692
0.80	.0113	.7667	.0204	.7661	.0310	.7705
0.85	.0116	.7680	.0212	.7673	.0323	.7718
0.90	.0120	.7692	.0219	.7685	.0336	.7731
0.95	.0124	.7704	.0227	.7696	.0349	.7743
1.00	.0128	.7716	.0235	.7707	.0362	.7755
1.10	.0136	.7738	.0251	.7728	.0390	.7778
1.20	.0144	.7760	.0267	.7749	.0420	.7800
1.30	.0152	.7781	.0285	.7768	.0451	.7822
1.40	.0160	.7801	.0304	.7787	.0485	.7842
1.50	.0169	.7821	.0323	.7805	.0521	.7862
1.60	.0178	.7840	.0344	.7822	.0559	.7881
1.70	.0188	.7858	.0366	.7838	.0600	.7899
1.80	.0198	.7875	.0390	.7854	.0644	.7916
1.90	.0209	.7892	.0415	.7868	.0691	.7932
2.00	.0220	.7909	.0442	.7882	.0740	.7947
2.10	.0232	.7924	.0471	.7896	.0793	.7961
2.20	.0245	.7939	.0502	.7908	.0848	.7974
2.30	.0258	.7954	.0534	.7920	.0906	.7986
2.40	.0272	.7968	.0569	.7931	.0967	.7997
2.50	.0287	.7981	.0605	.7941	.1030	.8006
2.60	.0303	.7994	.0643	.7950	.1096	.8015
2.70	.0320	.8007	.0684	.7958	.1164	.8022
2.80	.0338	.8018	.0726	.7966	.1235	.8027
2.90	.0357	.8029	.0770	.7972	.1307	.8031
3.00	.0376	.8040	.0816	.7977	.1382	.8034
3.10	.0397	.8050	.0863	.7981	.1458	.8035
3.20	.0420	.8059	.0913	.7985	.1536	.8035
3.30	.0443	.8068	.0964	.7987	.1615	.8033
3.40	.0467	.8076	.1017	.7987	.1695	.8029
3.50	.0493	.8083	.1071	.7987	.1777	.8024
3.60	.0519	.8089	.1127	.7986	.1860	.8017
3.70	.0547	.8095	.1184	.7983	.1944	.8008
3.80	.0576	.8100	.1242	.7979	.2028	.7998
3.90	.0605	.8105	.1302	.7973	.2113	.7985
4.00	.0636	.8108	.1362	.7967	.2199	.7971

depth	56K		170K		280K	
(um)	chi	Se	chi	Se	chi	Se
4.1	.0668	.8111	.1424	.7959	.2285	.7955
4.2	.0701	.8113	.1487	.7950	.2371	.7937
4.3	.0735	.8114	.1550	.7939	.2458	.7917
4.4	.0770	.8114	.1615	.7927	.2544	.7895
4.5	.0806	.8114	.1680	.7913	.2631	.7871
4.6	.0843	.8112	.1746	.7898	.2717	.7845
4.7	.0881	.8110	.1812	.7882	.2804	.7818
4.8	.0920	.8107	.1879	.7864	.2890	.7788
4.9	.0959	.8103	.1946	.7845	.2975	.7756
5.0	.1000	.8098	.2014	.7824	.3061	.7722
5.1	.1041	.8092	.2082	.7801	.3146	.7685
5.2	.1082	.8085	.2151	.7777	.3231	.7647
5.3	.1125	.8078	.2219	.7752	.3315	.7607
5.4	.1168	.8069	.2288	.7725	.3399	.7564
5.5	.1212	.8059	.2357	.7696	.3482	.7520
5.6	.1256	.8049	.2426	.7666	.3564	.7473
5.7	.1301	.8037	.2495	.7634	.3646	.7424
5.8	.1347	.8024	.2564	.7600	.3728	.7373
5.9	.1393	.8011	.2633	.7565	.3808	.7319
6.0	.1439	.7996	.2702	.7529	.3888	.7264
6.1	.1486	.7980	.2771	.7490	.3968	.7206
6.2	.1534	.7963	.2840	.7451	.4046	.7146
6.3	.1581	.7946	.2909	.7419	.4124	.7084
6.4	.1629	.7927	.2977	.7366	.4202	.7020
6.5	.1678	.7907	.3046	.7321	.4278	.6953
6.6	.1727	.7886	.3114	.7274	.4354	.6885
6.7	.1776	.7864	.3182	.7226	.4429	.6814
6.8	.1825	.7840	.3249	.7177	.4503	.6741
6.9	.1875	.7816	.3317	.7125	.4577	.6666
7.0	.1924	.7791	.3384	.7072	.4650	.6589

Theoretical dechanneling and electronic stopping power values for channeled 2.0 MeV protons in pure copper, ⟨100⟩.

depth	56K		170K		280K	
(um)	chi	Se	chi	Se	chi	Se
0.00	.0078	.6577	.0125	.6571	.0166	.6598
0.05	.0085	.6607	.0140	.6602	.0192	.6631
0.10	.0093	.6635	.0156	.6632	.0218	.6663
0.15	.0100	.6661	.0171	.6660	.0243	.6693
0.20	.0107	.6686	.0186	.6686	.0268	.6721
0.25	.0115	.6710	.0200	.6712	.0293	.6749
0.30	.0122	.6734	.0215	.6736	.0317	.6775
0.35	.0129	.6757	.0229	.6759	.0341	.6801
0.40	.0137	.6779	.0244	.6781	.0365	.6825
0.45	.0144	.6801	.0258	.6803	.0389	.6850
0.50	.0151	.6823	.0273	.6824	.0413	.6873
0.55	.0158	.6844	.0287	.6845	.0438	.6896
0.60	.0166	.6864	.0302	.6865	.0463	.6919
0.65	.0173	.6885	.0317	.6884	.0489	.6941
0.70	.0181	.6905	.0333	.6903	.0515	.6963
0.75	.0188	.6924	.0348	.6922	.0542	.6984
0.80	.0196	.6943	.0364	.6940	.0570	.7004
0.85	.0204	.6962	.0380	.6958	.0598	.7025
0.90	.0212	.6980	.0397	.6975	.0628	.7045
0.95	.0220	.6998	.0415	.6992	.0659	.7064
1.00	.0229	.7016	.0433	.7009	.0690	.7083
1.10	.0246	.7051	.0470	.7041	.0757	.7120
1.20	.0264	.7084	.0510	.7072	.0829	.7155
1.30	.0283	.7115	.0553	.7101	.0906	.7188
1.40	.0303	.7146	.0599	.7128	.0987	.7218
1.50	.0324	.7175	.0648	.7154	.1074	.7247
1.60	.0347	.7203	.0701	.7178	.1165	.7274
1.70	.0372	.7229	.0757	.7200	.1260	.7298
1.80	.0398	.7255	.0816	.7220	.1360	.7320
1.90	.0425	.7279	.0879	.7239	.1463	.7339
2.00	.0455	.7301	.0945	.7256	.1570	.7355
2.10	.0486	.7323	.1014	.7271	.1680	.7369
2.20	.0519	.7343	.1086	.7283	.1793	.7380
2.30	.0555	.7362	.1062	.7294	.1908	.7388
2.40	.0592	.7379	.1239	.7302	.2025	.7393
2.50	.0631	.7395	.1320	.7309	.2143	.7395
2.60	.0672	.7409	.1403	.7313	.2263	.7394
2.70	.0715	.7423	.1488	.7315	.2384	.7390
2.80	.0760	.7434	.1575	.7314	.2506	.7383
2.90	.0807	.7444	.1663	.7312	.2628	.7373
3.00	.0856	.7453	.1754	.7307	.2750	.7360
3.10	.0906	.7460	.1846	.7299	.2872	.7343
3.20	.0958	.7466	.1938	.7289	.2994	.7323
3.30	.1012	.7470	.2032	.7277	.3115	.7300
3.40	.1067	.7472	.2127	.7263	.3235	.7274
3.50	.1124	.7473	.2223	.7246	.3355	.7245
3.60	.1182	.7472	.2319	.7226	.3474	.7212
3.70	.1242	.7470	.2415	.7205	.3592	.7176
3.80	.1302	.7466	.2512	.7180	.3708	.7137
3.90	.1364	.7466	.2608	.7154	.3823	.7094
4.00	.1427	.7453	.2705	.7125	.3937	.7049

depth	56K		170K		280K	
(um)	chi	Se	chi	Se	chi	Se
4.1	.1491	.7444	.2802	.7093	.4050	.7000
4.2	.1556	.7433	.2898	.7059	.4161	.6948
4.3	.1622	.7421	.2995	.7023	.4270	.6892
4.4	.1688	.7407	.3091	.6984	.4378	.6833
4.5	.1755	.7392	.3186	.6943	.4485	.6771
4.6	.1823	.7374	.3281	.6899	.4589	.6706
4.7	.1891	.7356	.3375	.6853	.4693	.6637
4.8	.1959	.7335	.3469	.6805	.4794	.6566
4.9	.2028	.7313	.3562	.6754	.4894	.6491
5.0	.2098	.7289	.3655	.6700	.4993	.6413
5.1	.2167	.7264	.3747	.6645	.5090	.6332
5.2	.2237	.7236	.3838	.6586	.5185	.6247
5.3	.2308	.7208	.3928	.6526	.5279	.6160
5.4	.2378	.7177	.4017	.6463	.5371	.6070
5.5	.2448	.7145	.4106	.6398	.5462	.5976
5.6	.2519	.7111	.4194	.6330	.5551	.5880
5.7	.2589	.7076	.4280	.6260	.5639	.5781
5.8	.2660	.7039	.4367	.6188	.5726	.5679
5.9	.2730	.7000	.4452	.6114	.5811	.5574
6.0	.2801	.6960	.4536	.6037	.5995	.5466
6.1	.2871	.6918	.4620	.5958	.5978	.5356
6.2	.2941	.6875	.4702	.5877	.6059	.5243
6.3	.3011	.6829	.4784	.5793	.6139	.5127
6.4	.3081	.6783	.4865	.5707	.6218	.5009
6.5	.3150	.6734	.4945	.5620	.6295	.4888
6.6	.3220	.6684	.5024	.5530	.6372	.4765
6.7	.3289	.6633	.5103	.5438	.6447	.4639
6.8	.3358	.6580	.5180	.5344	.6522	.4511
6.9	.3427	.6525	.5257	.5248	.6595	.4381
7.0	.3495	.6469	.5333	.5150	.6667	.4248

February
1.0 MeV proton backscattering spectrum on copper.
Gr4 Sp4 ⟨100⟩ tilt 32.00 35 K 1.0 uC

30	1506	1505	1464	1472	1488	1480	1373	1449	1407	1426
40	1394	1380	1352	1326	1414	1252	1324	1250	1224	1361
50	1260	1294	1233	1193	1232	1218	1234	1184	1165	1136
60	1123	1137	1073	1082	1073	1066	1114	1021	1099	1018
70	1074	1058	972	991	988	1020	984	969	1004	937
80	929	959	943	923	912	860	828	874	873	858
90	802	807	823	788	790	782	748	767	759	708
100	681	683	700	684	686	657	618	688	643	669
110	635	628	561	550	592	584	582	591	571	561
120	545	512	511	537	476	480	446	488	475	478
130	451	453	451	447	432	399	392	412	365	411
140	398	365	375	331	359	338	328	314	301	311
150	309	304	312	304	291	282	287	274	246	273
160	260	265	219	219	223	216	206	203	221	207
170	198	181	176	152	159	169	149	182	175	155
180	159	139	152	123	116	121	135	103	125	104
190	107	118	106	105	97	86	74	84	83	99
200	153	112	30	2	2	0				

1.0 MeV proton backscattering spectrum on copper.
Gr6 Sp6 ⟨110⟩ tilt 16.63 35 K 1.0 uC

30	649	643	680	680	659	633	623	599	609	640
40	615	604	553	618	586	534	624	583	586	549
50	545	550	539	519	527	479	500	531	517	512
60	508	491	504	498	479	483	442	432	437	423
70	421	409	423	424	454	415	433	485	377	414
80	398	438	358	364	365	368	333	374	360	353
90	349	341	339	345	341	345	327	324	320	310
100	287	296	333	309	323	294	312	301	288	281
110	285	311	240	267	240	237	256	237	239	220
120	232	213	236	247	232	208	207	224	202	227
130	226	197	191	180	205	189	180	210	190	184
140	170	186	171	134	178	171	151	159	168	136
150	141	143	153	138	166	148	146	146	140	136
160	117	111	120	131	118	115	98	107	112	99
170	94	99	94	112	79	111	90	94	84	82
180	83	99	79	89	75	88	89	63	61	59
190	61	62	72	50	59	58	51	46	59	77
200	149	90	14	2	0	0				

1.0 MeV proton backscattering spectrum on copper.
Gr8 Sp8 ⟨110⟩ tilt 16.63 120 K 1.0 uC

30	1359	1323	1243	1304	1240	1256	1194	1219	1191	1174
40	1183	1192	1144	1167	1117	1116	1124	1094	1087	1088
50	1068	1102	1031	1042	1001	1075	1034	1042	921	949
60	995	960	933	861	905	856	924	880	932	901
70	895	841	848	885	807	821	818	822	795	823
80	767	781	767	777	722	757	743	730	699	662
90	707	682	656	627	647	648	694	643	673	601
100	639	626	583	620	579	560	548	532	554	553
110	531	523	535	520	506	469	472	487	487	466
120	421	420	459	463	426	451	450	406	400	379
130	375	409	371	366	328	343	332	356	335	355
140	299	337	318	293	307	284	269	287	252	291
150	250	214	245	243	231	248	278	217	231	230
160	218	201	203	214	190	177	207	189	182	182
170	165	189	173	148	139	154	153	163	153	141
180	138	140	139	129	115	118	126	102	121	100
190	100	95	103	97	86	87	78	74	89	90
200	146	123	34	3	1	1				

1.0 MeV proton backscattering spectrum on copper.
Gr10 Sp10 ⟨100⟩ tilt 32.00 120 K 1.0 uC

30	2605	2667	2643	2531	2637	2613	2522	2617	2441	2405
40	2369	2419	2369	2327	2399	2340	2306	2210	2351	2253
50	2298	2282	2313	2085	2167	2047	2041	2172	1952	1959
60	1978	1965	2002	1940	2005	1934	1878	1858	1866	1812
70	1812	1790	1887	1868	1747	1817	1747	1716	1675	1674
80	1643	1699	1655	1608	1595	1531	1532	1578	1529	1565
90	1421	1532	1479	1484	1402	1499	1388	1353	1302	1348
100	1339	1312	1271	1235	1258	1258	1270	1221	1250	1192
110	1163	1082	1103	1049	1093	1115	1060	1065	1057	972
120	995	979	963	939	916	890	928	897	826	854
130	786	755	806	760	774	729	751	700	728	714
140	663	622	670	632	624	589	595	592	546	549
150	566	552	535	492	543	501	515	466	425	447
160	427	418	411	407	376	348	368	389	321	336
170	327	330	303	325	284	290	269	286	245	229
180	208	212	251	221	200	203	193	184	179	167
190	169	162	138	138	130	138	108	120	120	119
200	159	143	57	11	3	5				

1.0 MeV proton backscattering spectrum on copper.
Grl2 Spl2 ⟨100⟩ tilt 32.00 200 K 1.0 uC

30	3766	3548	3714	3548	3602	3473	3542	3512	3489	3414
40	3314	3344	3346	3435	3312	3263	3189	3293	3204	3146
50	3200	3117	3118	3171	3172	2967	3020	3022	3081	2975
60	2999	2995	2888	2947	2914	2797	2967	2780	2839	2587
70	2752	2704	2676	2627	2603	2562	2768	2540	2450	2567
80	2490	2558	2579	2465	2380	2429	2310	2318	2378	2360
90	2283	2343	2199	2135	2209	2189	2176	2097	2099	2048
100	2027	2010	2035	2037	1955	1936	1921	1891	1853	1849
110	1782	1715	1830	1800	1759	1708	1652	1668	1640	1598
120	1559	1539	1532	1496	1434	1482	1458	1379	1386	1357
130	1365	1336	1322	1237	1242	1235	1229	1228	1197	1093
140	1157	1110	1114	1070	1013	946	961	924	883	867
150	916	856	813	827	862	831	781	773	786	746
160	698	701	691	626	657	592	575	593	577	565
170	575	522	510	479	493	448	407	399	437	414
180	363	407	358	313	313	294	288	286	279	248
190	265	230	244	220	210	221	187	186	184	189
200	240	155	47	14	4	3				

1.0 MeV proton backscattering spectrum on copper.
Grl3 Spl3 ⟨110⟩ tilt 16.62 200 K 1.0 uC

30	1980	1841	1860	1864	1905	1742	1883	1879	1761	1773
40	1776	1748	1755	1641	1711	1663	1639	1585	1676	1605
50	1589	1558	1560	1480	1526	1501	1511	1481	1537	1460
60	1422	1462	1481	1396	1376	1376	1429	1385	1285	1259
70	1306	1263	1332	1300	1293	1222	1253	1254	1223	1309
80	1179	1205	1161	1146	1140	1137	1153	1109	1043	1068
90	1039	1041	1081	1122	993	1046	1012	961	965	991
100	971	935	923	893	909	857	863	835	850	857
110	896	781	733	738	783	755	734	753	678	717
120	721	697	611	615	644	684	654	627	613	626
130	628	606	586	518	528	524	522	516	454	529
140	495	462	456	486	428	419	443	389	417	362
150	437	389	413	391	407	372	380	330	357	348
160	333	284	181	309	296	279	257	263	260	252
170	229	259	281	239	250	217	216	196	193	194
180	197	181	170	160	165	175	184	165	148	146
190	147	142	136	121	127	127	118	114	118	111
200	159	123	33	13	4	2				

1.0 MeV proton backscattering spectrum on copper.
Gr14 Sp14 ⟨110⟩ tilt 16.62 280 K 1.0 uC

30	2626	2636	2562	2571	2504	2540	2501	2375	2375	2382
40	2412	2403	2473	2350	2309	2365	2276	2239	2298	2210
50	2231	2237	2174	2201	2175	2110	2095	2067	2080	2106
60	1988	2100	1965	2041	2011	1958	1934	1850	1966	1987
70	1814	1948	1848	1839	1898	1758	1823	1859	1743	1772
80	1714	1695	1698	1721	1578	1615	1625	1647	1641	1483
90	1541	1556	1435	1446	1455	1415	1446	1456	1347	1378
100	1387	1344	1356	1314	1341	1302	1278	1235	1259	1240
110	1209	1232	1190	1140	1110	1117	1093	1065	1088	1052
120	1025	973	1030	990	966	921	947	851	902	886
130	910	848	843	772	815	789	857	846	711	743
140	728	747	700	659	705	655	663	661	630	550
150	599	565	624	568	549	534	535	525	503	455
160	460	488	495	453	397	390	378	393	359	407
170	323	329	362	332	319	322	338	288	247	281
180	337	251	232	228	241	243	218	236	207	228
190	203	181	167	162	159	159	163	159	142	151
200	?150	125	51	10	4	3				

1.0 MeV proton backscattering spectrum on copper.
Gr15 Sp15 ⟨100⟩ tilt 31.96 280 K 1.0 uC

30	4486	4368	4417	4443	4552	4523	4365	4349	4331	4319
40	4223	4246	4229	4088	4099	4069	4045	3995	4060	3962
50	4057	4147	3981	3817	3930	4004	3815	3767	3656	3659
60	3746	3760	3557	3629	3631	3595	3583	3645	3529	3483
70	3405	3483	3451	3450	3294	3283	3366	3308	3366	3198
80	3136	3126	3135	3203	3062	3119	3120	2965	3003	2988
90	3010	2987	3000	2931	2872	2815	2772	2766	2695	2714
100	2671	2575	2660	2637	2640	2512	2523	2565	2513	2417
110	2454	2379	2330	2327	2254	2266	2218	2145	2192	2103
120	2195	2029	2127	2053	1953	1967	1914	1910	1921	1849
130	1766	1802	1766	1793	1632	1703	1615	1673	1530	1551
140	1550	1478	1455	1457	1418	1344	1340	1319	1238	1319
150	1281	1152	1141	1143	1170	1133	1037	1000	984	1019
160	958	967	912	926	845	862	828	739	785	806
170	715	710	682	702	671	640	602	579	536	537
180	516	487	495	436	466	417	400	422	368	359
190	356	337	304	258	293	278	220	233	240	269
200	249	164	71	15	9	7				

1.0 MeV proton backscattering spectrum on copper.
Gr4 Spl8 random rotating tilt 20.00 35 K 0.1 uC

30	907	829	864	876	820	862	859	848	884	794
40	848	858	841	785	807	855	804	783	825	839
50	792	799	814	794	845	838	855	713	815	816
60	759	791	798	796	791	798	800	770	825	780
70	768	776	741	828	729	752	788	783	781	740
80	759	775	739	736	746	818	753	736	794	680
90	763	745	726	750	741	764	707	746	693	759
100	716	746	740	772	749	689	726	713	759	694
110	774	726	768	702	704	726	724	687	741	711
120	721	691	669	688	676	693	701	679	727	727
130	703	723	642	713	751	690	711	678	711	743
140	653	689	677	665	653	672	666	629	696	696
150	681	716	705	679	644	674	659	664	664	708
160	675	673	726	678	685	611	655	649	688	673
170	624	639	615	659	621	674	620	631	601	612
180	633	577	656	645	637	636	665	665	607	664
190	565	592	637	623	590	590	612	616	577	575
200	377	182	58	10	6	2				

Dechanneling Fraction Cu#2 <110> 35K

Sc = 0.5 Sr		Sc = 0.85 Sr	
Depth (um)	Chi (%)	Depth (um)	Chi (%)
0.106	0.90	0.088	0.86
0.210	1.02	0.176	1.02
0.339	1.16	0.283	1.15
0.467	1.39	0.390	1.38
0.592	1.51	0.494	1.50
0.716	1.56	0.598	1.54
0.838	1.69	0.699	1.66
0.958	1.84	0.800	1.80
1.08	2.26	0.898	2.21
1.19	2.32	0.996	2.26
1.31	2.48	1.09	2.41
1.42	2.67	1.19	2.58
1.53	2.96	1.29	2.85
1.64	3.10	1.37	2.98
1.75	3.32	1.46	3.18
1.85	3.70	1.55	3.51
1.96	3.68	1.63	3.50
2.06	4.15	1.72	3.93
2.16	4.68	1.80	4.38
2.26	4.83	1.88	4.51
2.36	5.12	1.97	4.75
2.45	5.41	2.04	4.99
2.54	5.63	2.12	5.18
2.63	6.11	2.20	5.58
2.72	6.89	2.27	6.14
2.81	6.83	2.35	6.17
2.90	6.96	2.42	6.27
2.98	8.02	2.49	7.14
3.06	8.15	2.56	7.23
3.14	8.71	2.62	7.67
3.22	9.33	2.69	8.16
3.30	9.70	2.75	8.44
3.37	10.08	2.81	8.72
3.45	10.83	2.88	9.29

Dechanneling Fraction Cu#2 ⟨110⟩ 120K

Sc = 0.5 Sr		Sc = 0.85 Sr	
Depth (um)	Chi (%)	Depth (um)	Chi (%)
0.106	1.41	0.088	1.40
0.210	1.62	0.176	1.61
0.339	1.82	0.283	1.81
0.467	2.17	0.390	2.15
0.592	2.51	0.494	2.48
0.716	2.66	0.598	2.62
0.838	2.99	0.699	2.94
0.958	3.17	0.800	3.11
1.08	3.80	0.898	3.71
1.19	3.68	0.996	3.60
1.31	4.40	1.09	4.27
1.42	4.98	1.19	4.80
1.53	5.38	1.29	5.17
1.64	5.79	1.37	5.54
1.75	6.58	1.46	6.25
1.85	7.03	1.55	6.65
1.96	7.49	1.63	7.06
2.06	8.22	1.72	7.70
2.16	8.75	1.80	8.16
2.26	9.63	1.88	8.93
2.36	10.41	1.97	9.59
2.45	10.55	2.04	9.70
2.54	11.47	2.12	10.48
2.63	12.25	2.20	11.13
2.72	13.10	2.27	11.83
2.81	13.86	2.35	12.45
2.90	14.33	2.42	12.82
2.98	15.06	2.49	13.40
3.06	16.28	2.56	14.37
3.14	17.17	2.62	15.07
3.22	17.93	2.69	15.65
3.30	19.05	2.75	16.51
3.37	19.71	2.81	17.00
3.45	21.31	2.88	18.23

Dechanneling Fraction Cu#2 ⟨110⟩ 200K

Sc = 0.5 Sr		Sc = 0.85 Sr	
Depth (um)	Chi (%)	Depth (um)	Chi (%)
0.106	2.00	0.088	1.99
0.210	2.27	0.176	2.26
0.339	2.63	0.283	2.62
0.467	2.85	0.390	2.83
0.592	3.33	0.494	3.30
0.716	4.13	0.598	4.06
0.838	4.19	0.699	4.12
0.958	4.67	0.800	4.58
1.08	5.67	0.898	5.52
1.19	6.45	0.996	6.26
1.31	6.46	1.09	6.26
1.42	7.47	1.19	7.20
1.53	7.96	1.29	7.65
1.64	9.02	1.37	8.61
1.75	10.1	1.46	9.62
1.85	10.6	1.55	9.99
1.96	11.5	1.63	10.81
2.06	12.4	1.72	11.58
2.16	13.6	1.80	12.69
2.26	14.7	1.88	13.59
2.36	15.9	1.97	14.66
2.45	16.9	2.04	15.48
2.54	17.6	2.12	16.09
2.63	18.8	2.20	17.03
2.72	20.1	2.27	18.18
2.81	21.1	2.35	18.91
2.90	21.4	2.42	19.19
2.98	23.1	2.49	20.56
3.06	24.2	2.56	21.40
3.14	25.1	2.62	22.10
3.22	26.5	2.69	23.15
3.30	28.3	2.75	24.51
3.37	29.5	2.81	25.44
3.45	30.9	2.88	26.51

Dechanneling Fraction Cu#2 <110> 280K

Sc = 0.5 Sr		Sc = 0.85 Sr	
Depth (um)	Chi (%)	Depth (um)	Chi (%)
0.106	2.64	0.088	2.63
0.210	2.94	0.176	2.92
0.339	3.66	0.283	3.63
0.467	4.23	0.390	4.19
0.592	4.85	0.494	4.79
0.716	5.45	0.598	5.37
0.838	6.18	0.699	6.07
0.958	7.18	0.800	7.02
1.08	8.10	0.898	7.89
1.19	9.21	0.996	8.93
1.31	10.12	1.09	9.78
1.42	11.41	1.19	10.97
1.53	12.43	1.29	11.91
1.64	13.18	1.37	12.58
1.75	14.21	1.46	13.51
1.85	16.07	1.55	15.17
1.96	17.12	1.63	16.11
2.06	18.54	1.72	17.35
2.16	20.21	1.80	18.81
2.26	21.32	1.88	19.76
2.36	22.43	1.97	20.70
2.45	23.68	2.04	21.75
2.54	25.62	2.12	23.39
2.63	27.27	2.20	24.53
2.72	28.73	2.27	25.96
2.81	30.26	2.35	27.20
2.90	30.80	2.42	27.59
2.98	32.60	2.49	29.03
3.06	33.56	2.56	29.76
3.14	35.79	2.62	31.52
3.22	36.62	2.69	32.12
3.30	38.73	2.75	33.74
3.37	39.06	2.81	33.93
3.45	41.67	2.88	35.92

Dechanneling Fraction Cu#2 ⟨100⟩ 35K

Sc = 0.5 Sr		Sc = 0.75 Sr	
Depth (um)	Chi (%)	Depth (um)	Chi (%)
0.106	1.44	0.093	1.44
0.210	1.80	0.184	1.79
0.340	1.89	0.297	1.88
0.467	2.25	0.409	2.23
0.593	2.73	0.519	2.71
0.716	2.82	0.627	2.80
0.838	3.37	0.734	3.32
0.959	3.70	0.840	3.65
1.08	4.32	0.943	4.24
1.19	4.80	1.05	4.70
1.31	5.07	1.15	4.95
1.42	5.90	1.24	5.73
1.53	6.18	1.34	5.99
1.64	7.05	1.44	6.80
1.75	7.46	1.53	7.18
1.86	8.30	1.62	7.96
1.96	9.19	1.72	8.77
2.06	9.26	1.81	8.83
2.16	10.40	1.89	9.86
2.26	10.84	1.98	10.25
2.36	12.02	2.06	11.31
2.45	12.81	2.15	12.00
2.54	13.73	2.23	12.82
2.64	15.16	2.31	14.07
2.72	15.77	2.39	14.59
2.81	16.41	2.46	15.14
2.90	12.99	2.54	12.12
2.98	17.80	2.61	16.29
3.06	19.29	2.68	17.56
3.14	20.36	2.75	18.45
3.22	20.99	2.82	18.96
3.30	22.72	2.89	20.40
3.38	23.46	2.96	20.99
3.45	24.45	3.02	21.79

Dechanneling Fraction Cu#2 ⟨100⟩ 120K

Sc = 0.5 Sr		Sc = 0.75 Sr	
Depth (um)	Chi (%)	Depth (um)	Chi (%)
0.106	2.06	0.093	2.05
0.210	2.49	0.184	2.48
0.340	3.00	0.297	2.98
0.467	3.58	0.409	3.55
0.593	4.35	0.519	4.30
0.716	5.15	0.627	5.09
0.838	5.65	0.734	5.57
0.959	6.40	0.840	6.30
1.08	7.50	0.943	7.35
1.19	8.50	1.05	8.34
1.31	9.19	1.15	8.96
1.42	10.4	1.24	10.08
1.53	11.4	1.34	11.02
1.64	12.3	1.44	11.83
1.75	14.0	1.53	13.40
1.86	15.5	1.62	14.82
1.96	16.8	1.72	16.04
2.06	17.3	1.81	16.42
2.16	20.0	1.89	18.89
2.26	20.4	1.98	19.23
2.36	22.1	2.06	20.74
2.45	23.4	2.15	21.94
2.54	24.8	2.23	23.11
2.64	26.6	2.31	24.69
2.72	27.6	2.39	25.57
2.81	29.4	2.46	27.12
2.90	29.8	2.54	27.43
2.98	32.1	2.61	29.35
3.06	32.7	2.68	29.87
3.14	36.5	2.75	33.08
3.22	37.5	2.82	33.86
3.30	39.0	2.89	35.10
3.38	41.3	2.96	36.96
3.45	42.8	3.02	38.21

Dechanneling Fraction Cu#2 ⟨100⟩ 200K

Sc = 0.5 Sr		Sc = 0.75 Sr	
Depth (um)	Chi (%)	Depth (um)	Chi (%)
0.106	3.29	0.093	3.28
0.210	3.95	0.184	3.93
0.340	4.50	0.297	4.48
0.467	5.75	0.409	5.71
0.593	6.94	0.519	6.87
0.716	8.48	0.627	8.37
0.838	9.33	0.734	9.19
0.959	10.62	0.840	10.44
1.08	12.50	0.943	12.24
1.19	13.57	1.05	13.25
1.31	14.66	1.15	14.28
1.42	17.73	1.24	17.19
1.53	18.84	1.34	18.23
1.64	20.60	1.44	19.86
1.75	22.39	1.53	21.51
1.86	24.38	1.62	23.35
1.96	26.31	1.72	25.11
2.06	27.94	1.81	26.59
2.16	30.3	1.89	28.72
2.26	31.9	1.98	30.10
2.36	33.8	2.06	31.82
2.45	35.5	2.15	33.35
2.54	37.5	2.23	35.09
2.64	40.2	2.31	37.41
2.72	40.8	2.39	37.95
2.81	42.6	2.46	39.49
2.90	44.1	2.54	40.73
2.98	47.4	2.61	43.49
3.06	47.9	2.68	43.92
3.14	50.7	2.75	46.24
3.22	51.5	2.82	46.87
3.30	53.9	2.89	48.82
3.38	55.7	2.96	50.26
3.45	58.2	3.02	52.24

Dechanneling Fraction Cu#2 ⟨100⟩ 280K

Sc = 0.5 Sr		Sc = 0.75 Sr	
Depth (um)	Chi (%)	Depth (um)	Chi (%)
0.106	3.9	0.093	3.92
0.210	5.2	0.184	5.21
0.339	6.4	0.297	6.34
0.467	7.9	0.409	7.82
0.592	9.5	0.519	9.45
0.716	11.4	0.627	11.29
0.838	12.9	0.734	12.75
0.958	14.5	0.840	14.26
1.08	16.5	0.943	16.14
1.19	18.7	1.05	18.27
1.31	21.1	1.15	20.51
1.42	23.9	1.24	23.14
1.53	25.4	1.34	24.57
1.64	27.7	1.44	26.73
1.75	30.3	1.53	29.11
1.86	33.4	1.62	32.00
1.96	34.7	1.72	33.12
2.06	36.8	1.81	35.06
2.16	40.1	1.89	38.03
2.26	41.6	1.98	39.32
2.36	43.6	2.06	41.15
2.45	47.0	2.15	44.14
2.54	48.1	2.23	45.03
2.64	50.0	2.31	46.70
2.72	52.0	2.39	48.44
2.81	54.2	2.46	50.26
2.90	55.9	2.54	51.74
2.98	58.2	2.61	53.62
3.06	59.5	2.68	54.72
3.14	63.5	2.75	58.09
3.22	63.8	2.82	58.19
3.30	66.5	2.89	60.38
3.38	69.3	2.96	62.68
3.45	70.1	3.02	63.24

April
1MeV proton backscattering spectra on Cu(.01%In)
Gr3 Sp17 ⟨100⟩ tilt 36.63 35 K 1.0 uC

30	1696	1637	1693	1697	1615	1719	1594	1671	1601	1590
40	1569	1492	1530	1455	1464	1492	1423	1465	1472	1488
50	1430	1393	1417	1431	1326	1358	1353	1274	1261	1261
60	1275	1257	1295	1265	1188	1231	1230	1218	1132	1050
70	1150	1172	1123	1107	1183	1117	1064	1099	1076	1027
80	1048	985	1019	1036	963	982	946	939	865	916
90	898	918	854	912	922	833	803	809	817	816
100	759	798	789	785	778	735	686	729	706	709
110	697	660	664	665	704	639	676	626	606	588
120	581	603	562	629	554	577	525	474	507	479
130	500	486	451	485	445	474	420	467	419	457
140	414	426	394	405	391	380	359	381	371	391
150	318	311	341	351	327	309	300	303	284	293
160	286	281	297	263	251	237	247	253	208	231
170	202	219	200	208	187	181	184	198	198	171
180	193	165	150	153	154	164	131	106	144	127
190	136	121	131	118	91	88	92	86	89	96
200	159	169	138	39	8	0	0			

1MeV proton backscattering spectra on Cu(.01%In)
Gr4 Sp18 ⟨110⟩ tilt 29.70 35 K 1.0 uC

30	811	852	853	857	842	810	813	799	783	778
40	767	813	738	783	694	698	702	770	688	705
50	676	718	672	671	671	737	608	656	648	623
60	632	557	604	599	606	587	601	596	562	531
70	576	534	543	589	578	535	541	560	504	557
80	502	523	461	480	508	462	452	414	471	477
90	475	471	431	464	446	429	432	445	419	367
100	417	407	428	371	389	357	378	341	359	326
110	343	365	339	325	359	330	306	322	347	277
120	331	348	269	298	315	279	304	285	263	260
130	260	279	243	259	257	261	236	235	278	236
140	220	225	253	202	202	206	209	206	217	211
150	182	197	172	180	191	203	199	170	162	174
160	152	181	148	164	166	153	124	141	141	140
170	162	128	126	122	98	126	87	115	113	101
180	103	98	113	84	83	82	101	97	82	72
190	106	69	81	68	56	53	70	47	59	82
200	116	166	132	35	4	1	0			

1MeV proton backscattering spectra on Cu(.01%In)
Gr4 Sp10 ⟨110⟩ tilt 29.66 120 K 1.0 uC

30	1350	1415	1322	1382	1371	1313	1364	1304	1298	1268
40	1176	1237	1292	1189	1179	1250	1241	1171	1178	1137
50	1133	1092	1129	1120	1120	1126	1088	1101	1062	1015
60	1023	1015	1021	1062	994	951	980	1005	960	949
70	1002	929	958	929	890	921	914	870	872	851
80	846	820	887	882	801	815	817	783	761	803
90	773	751	758	768	749	678	695	654	748	655
100	726	664	663	645	632	650	638	639	655	592
110	612	543	559	538	526	523	555	530	506	530
120	519	489	461	504	443	482	460	431	406	462
130	435	452	415	448	400	442	382	365	377	379
140	380	367	359	373	367	332	356	350	319	308
150	320	327	326	296	281	279	308	262	266	260
160	261	233	241	230	266	249	229	219	216	215
170	223	217	183	197	184	178	171	187	173	145
180	161	192	154	143	143	154	115	136	126	127
190	125	109	94	118	87	129	90	110	87	110
200	162	189	154	48	12	3	1			

1MeV proton backscattering spectra on Cu(.01%In)
Gr5 Sp11 ⟨100⟩ tilt 36.63 120 K 1.0 uC

30	2689	2577	2609	2682	2581	2645	2536	2537	2446	2467
40	2462	2487	2439	2315	2344	2278	2299	2376	2307	2252
50	2384	2182	2148	2258	2206	2227	2107	2143	2095	2165
60	2066	2071	2081	2010	1986	2027	1930	1974	1920	1870
70	1876	1848	1879	1859	1754	1880	1714	1733	1745	1731
80	1701	1635	1658	1647	1625	1599	1627	1559	1545	1576
90	1501	1474	1498	1507	1445	1405	1424	1392	1480	1310
100	1376	1329	1318	1214	1324	1274	1219	1275	1259	1184
110	1192	1174	1145	1139	1057	1098	1068	1068	1018	1038
120	1001	986	969	952	966	889	948	893	859	843
130	794	834	838	805	840	749	778	749	712	711
140	692	695	653	629	684	607	588	626	547	546
150	593	510	507	510	514	493	523	474	473	417
160	408	440	439	426	405	391	400	416	391	360
170	348	335	328	322	316	308	304	300	241	275
180	276	239	221	228	216	207	215	198	195	200
190	162	190	163	143	160	157	151	137	132	147
200	174	224	159	51	13	5	1			

1MeV proton backscattering spectra on Cu(.01%In)
Gr6 Spl2 ⟨100⟩ tilt 36.63 200 K 1.0 uC

30	3788	3659	3727	3711	3563	3591	3535	3472	3547	3433
40	3522	3510	3362	3381	3288	3330	3278	3272	3239	3283
50	3242	3343	3107	3193	3045	3135	3080	3027	2971	2887
60	3085	3043	2949	3029	2851	2965	2843	2819	2899	2679
70	2740	2722	2768	2637	2617	2714	2640	2542	2607	2535
80	2528	2511	2497	2457	2484	2406	2412	2395	2298	2350
90	2270	2195	2220	2255	2207	2134	2122	2110	2137	2132
100	2076	2013	2065	1972	1944	1945	1928	1834	1907	1770
110	1772	1787	1725	1800	1746	1670	1649	1618	1589	1595
120	1517	1572	1500	1523	1485	1419	1380	1405	1341	1374
130	1274	1318	1290	1210	1268	1198	1175	1155	1167	1087
140	1084	1095	1045	996	1012	991	963	899	852	937
150	908	828	820	837	788	763	807	755	711	709
160	679	729	657	656	657	670	584	572	552	507
170	557	519	535	522	483	450	404	400	400	389
180	368	362	363	344	333	339	338	299	299	295
190	253	277	264	252	225	189	206	182	195	188
200	242	264	190	55	6	2	3			

1MeV proton backscattering spectra on Cu(.01%In)
Gr7 Spl3 ⟨110⟩ tilt 29.70 200 K 1.0 uC

30	2192	2105	2139	2131	2119	2150	2161	2010	2030	2036
40	1988	1951	1926	1977	1887	1910	1876	1889	1890	1876
50	1738	1816	1815	1778	1872	1816	1723	1689	1678	1694
60	1670	1674	1654	1581	1657	1545	1495	1560	1553	1542
70	1540	1471	1493	1532	1536	1462	1425	1441	1375	1345
80	1422	1360	1406	1323	1322	1320	1333	1252	1265	1320
90	1174	1219	1186	1174	1163	1127	1069	1130	1114	1103
100	1083	1109	1087	1022	1009	989	957	992	928	965
110	958	920	889	928	873	875	894	830	868	825
120	760	783	807	776	751	726	753	707	697	720
130	743	673	701	723	625	666	656	622	600	587
140	597	546	584	544	565	525	523	519	487	482
150	467	460	468	430	449	458	439	431	424	390
160	411	385	383	387	343	368	318	326	345	335
170	330	311	283	292	289	257	281	234	255	260
180	249	269	231	227	190	206	219	195	173	154
190	194	156	172	168	178	147	145	133	154	142
200	204	218	155	67	11	3	1			

1MeV proton backscattering spectra on Cu(.01%In)
Gr1 Spl4 ⟨100⟩ tilt 36.63 280 K 1.0 uC

30	4630	4504	4626	4520	4477	4454	4395	4380	4431	4276
40	4314	4312	4271	4305	4077	4121	4063	4090	3994	3999
50	4086	3929	4105	4002	3998	3938	3821	3846	3739	3909
60	3754	3787	3662	3559	3660	3724	3593	3603	3516	3648
70	3481	3479	3432	3522	3443	3368	3403	3337	3327	3256
80	3299	3289	3282	3145	3197	3178	3088	3187	3091	3007
90	3132	3042	3035	2947	2912	2977	2876	2865	2806	2733
100	2688	2752	2743	2799	2709	2693	2676	2620	2494	2543
110	2452	2449	2405	2448	2280	2309	2343	2185	2208	2243
120	2224	2141	2158	2049	2031	2091	1964	1892	1869	1875
130	1812	1748	1837	1699	1727	1713	1628	1599	1573	1573
140	1596	1573	1478	1378	1344	1380	1296	1285	1253	1201
150	1236	1220	1145	1123	1124	1098	1065	1115	951	977
160	945	956	886	880	809	855	817	803	806	741
170	706	685	682	650	689	650	626	542	596	562
180	544	526	491	452	465	446	442	424	401	374
190	362	359	348	331	269	311	218	267	240	264
200	237	315	208	52	16	8	11			

1MeV proton backscattering spectra on Cu(.01%In)
Gr2 Spl6 ⟨110⟩ tilt 29.70 280 K 1.0 uC

30	2946	2862	2839	2854	2859	2841	2804	2792	2697	2748
40	2780	2643	2555	2651	2585	2534	2509	2565	2508	2495
50	2475	2434	2519	2334	2381	2374	2324	2280	2328	2325
60	2254	2268	2280	2271	2209	2233	2176	2182	2121	1991
70	2088	2060	2003	1964	1996	1921	2002	1904	1938	1906
80	1852	1932	1847	1957	1857	1864	1855	1834	1760	1650
90	1772	1660	1704	1656	1728	1628	1609	1670	1574	1602
100	1574	1440	1468	1484	1522	1417	1466	1433	1423	1320
110	1367	1339	1339	1325	1295	1239	1304	1225	1237	1173
120	1210	1146	1100	1135	1115	1143	1072	1048	968	1020
130	995	993	928	968	976	916	914	851	826	868
140	836	813	821	792	779	723	776	731	742	690
150	702	671	652	608	614	587	605	640	570	572
160	507	571	549	518	473	539	431	481	484	457
170	425	407	396	380	378	364	369	322	373	346
180	316	293	321	315	277	303	276	251	209	228
190	260	241	205	198	193	200	192	170	175	181
200	252	231	871	65	8	5	3			

1MeV proton backscattering spectra on Cu(.01%In)
Gr6 Sp19 random rotating tilt 20.00 35 K 0.1 uC

30	906	964	898	925	851	872	929	904	952	898
40	846	827	898	870	858	898	795	880	826	846
50	873	847	898	811	827	798	828	826	845	794
60	841	792	867	797	841	831	868	787	804	821
70	794	793	835	857	842	807	781	815	780	827
80	843	822	766	856	765	815	810	831	772	822
90	803	794	761	781	758	782	783	783	741	784
100	769	799	769	786	782	785	785	743	793	714
110	787	758	763	751	736	772	744	724	777	701
120	768	715	732	743	734	748	738	728	712	720
130	752	735	731	765	758	752	730	706	689	740
140	722	713	775	707	659	720	721	689	676	673
150	690	700	709	711	687	710	709	746	703	774
160	666	721	670	693	708	672	711	650	679	699
170	684	701	698	644	690	668	670	668	657	664
180	658	671	681	661	669	691	639	653	597	663
190	606	634	656	627	640	644	652	645	602	647
200	527	375	148	38	9	1	1			

Dechanneling Fraction Cu(.01In) <110> 35K

Sc = 0.5 Sr		Sc = 0.85 Sr	
Depth (um)	Chi (%)	Depth (um)	Chi (%)
0.08	0.9	0.088	0.90
0.21	1.2	0.176	1.20
0.34	1.4	0.283	1.34
0.47	1.5	0.390	1.46
0.59	1.7	0.494	1.64
0.72	1.9	0.598	1.90
0.84	2.1	0.699	2.08
0.96	2.4	0.800	2.40
1.08	2.7	0.898	2.59
1.19	2.8	0.996	2.68
1.31	3.2	1.09	3.07
1.42	3.3	1.19	3.16
1.53	3.7	1.29	3.56
1.64	3.8	1.37	3.62
1.75	4.1	1.46	3.95
1.85	4.6	1.55	4.39
1.96	4.7	1.63	4.43
2.06	5.1	1.72	4.81
2.16	5.2	1.80	4.84
2.26	5.9	1.88	5.51
2.36	6.2	1.97	5.76
2.45	6.8	2.04	6.26
2.54	6.6	2.12	6.09
2.64	7.3	2.20	6.66
2.72	8.1	2.27	7.35
2.81	8.4	2.35	7.53
2.90	8.6	2.42	7.71
2.98	9.0	2.49	8.03
3.06	10.0	2.56	8.88
3.14	10.3	2.62	9.10
3.22	10.9	2.69	9.57
3.30	11.7	2.75	10.18
3.37	12.0	2.81	10.41
3.45	12.9	2.88	11.06

Dechanneling Fraction Cu(.01In) ⟨110⟩ 120K

Sc = 0.5 Sr		Sc = 0.85 Sr	
Depth (um)	Chi (%)	Depth (um)	Chi (%)
0.08	1.6	0.088	1.58
0.21	1.7	0.176	1.68
0.34	2.1	0.283	2.04
0.47	2.4	0.390	2.40
0.59	2.6	0.494	2.58
0.72	3.0	0.598	2.99
0.84	3.4	0.699	3.35
0.96	3.7	0.800	3.64
1.08	4.0	0.898	3.89
1.19	4.6	0.996	4.52
1.31	5.0	1.09	4.87
1.42	5.5	1.19	5.70
1.53	5.8	1.29	5.55
1.64	6.3	1.37	6.00
1.75	6.7	1.46	6.36
1.85	7.1	1.55	6.78
1.96	7.8	1.63	7.41
2.06	8.2	1.72	7.72
2.16	9.4	1.80	8.78
2.26	9.8	1.88	9.12
2.36	10.2	1.97	9.45
2.45	11.3	2.04	10.41
2.54	11.7	2.12	10.71
2.64	12.6	2.20	11.45
2.72	13.3	2.27	12.07
2.81	14.0	2.35	12.60
2.90	14.5	2.42	13.00
2.98	15.4	2.49	13.74
3.06	16.5	2.56	14.64
3.14	16.9	2.62	14.93
3.22	18.4	2.69	16.08
3.30	18.6	2.75	16.24
3.37	19.8	2.81	17.11
3.45	20.8	2.88	17.92

Dechanneling Fraction Cu(.01In) ⟨110⟩ 200K

Sc = 0.5 Sr		Sc = 0.85 Sr	
Depth (um)	Chi (%)	Depth (um)	Chi (%)
0.08	2.3	0.088	2.27
0.21	2.7	0.176	2.74
0.34	2.9	0.283	2.93
0.47	3.6	0.390	3.53
0.59	3.9	0.494	3.89
0.72	4.5	0.598	4.49
0.84	5.1	0.699	5.03
0.96	5.8	0.800	5.64
1.08	6.3	0.898	6.12
1.19	6.8	0.996	6.62
1.31	7.7	1.09	7.43
1.42	8.4	1.19	8.15
1.53	9.3	1.29	8.96
1.64	10.2	1.37	9.71
1.75	10.7	1.46	10.24
1.85	11.5	1.55	10.90
1.96	12.8	1.63	12.06
2.06	13.6	1.72	12.73
2.16	14.3	1.80	13.35
2.26	15.7	1.88	14.57
2.36	16.5	1.97	15.30
2.45	17.6	2.04	16.21
2.54	19.2	2.12	17.53
2.64	20.4	2.20	18.51
2.72	21.2	2.27	19.22
2.81	22.6	2.35	20.30
2.90	23.0	2.42	20.67
2.98	24.9	2.49	22.18
3.06	26.4	2.56	23.37
3.14	27.4	2.62	24.13
3.22	29.0	2.69	25.39
3.30	29.9	2.75	26.06
3.37	31.4	2.81	27.15
3.45	32.5	2.88	27.95

Dechanneling Fraction Cu(.01In) ⟨110⟩ 280K

Sc = 0.5 Sr		Sc = 0.85 Sr	
Depth (um)	Chi (%)	Depth (um)	Chi (%)
0.08	2.9	0.088	2.89
0.21	3.5	0.176	3.46
0.34	3.9	0.283	3.92
0.47	4.6	0.390	4.61
0.59	5.4	0.494	5.37
0.72	6.0	0.598	5.92
0.84	7.3	0.699	7.12
0.96	7.9	0.800	7.74
1.08	8.7	0.898	8.51
1.19	9.7	0.996	9.47
1.31	11.1	1.09	10.73
1.42	12.1	1.19	11.63
1.53	13.1	1.29	12.53
1.64	14.3	1.37	13.63
1.75	15.7	1.46	14.95
1.85	17.0	1.55	16.08
1.96	18.5	1.63	17.38
2.06	19.9	1.72	18.60
2.16	20.9	1.80	19.54
2.26	22.1	1.88	20.54
2.36	24.2	1.97	22.35
2.45	25.4	2.04	23.36
2.54	26.4	2.12	24.17
2.64	28.0	2.20	25.54
2.72	29.0	2.27	26.33
2.81	29.9	2.35	26.97
2.90	32.0	2.42	28.72
2.98	34.0	2.49	30.31
3.06	35.5	2.56	31.51
3.14	36.6	2.62	32.36
3.22	38.5	2.69	33.77
3.30	40.4	2.75	35.29
3.37	41.6	2.81	36.09
3.45	43.3	2.88	37.39

Dechanneling Fraction Cu(.01In) <100> 35K

Sc = 0.5 Sr		Sc = 0.75 Sr	
Depth (um)	Chi (%)	Depth (um)	Chi (%)
0.08	1.4	0.093	1.40
0.21	1.9	0.184	1.88
0.34	2.1	0.297	2.08
0.47	2.5	0.409	2.48
0.59	2.9	0.519	2.83
0.72	3.1	0.627	3.04
0.84	3.6	0.734	3.52
0.96	4.2	0.840	4.10
1.08	4.3	0.943	4.27
1.19	5.0	1.05	4.86
1.31	5.7	1.15	5.55
1.42	6.1	1.24	5.91
1.53	6.6	1.34	6.45
1.64	6.9	1.44	6.70
1.75	7.7	1.53	7.38
1.85	8.7	1.62	8.37
1.96	9.4	1.72	8.95
2.06	10.1	1.81	9.61
2.16	10.5	1.89	10.02
2.26	11.6	1.98	10.92
2.36	12.2	2.06	11.46
2.45	13.6	2.15	12.70
2.54	13.8	2.23	12.88
2.64	15.1	2.31	14.08
2.72	16.2	2.39	15.02
2.81	17.2	2.46	15.87
2.90	17.7	2.54	16.26
2.98	19.1	2.61	17.48
3.06	20.1	2.68	18.27
3.14	21.4	2.75	19.42
3.22	22.7	2.82	20.50
3.30	23.2	2.89	20.87
3.37	24.9	2.96	22.28
3.45	25.5	3.02	22.72

Dechanneling Fraction Cu(.01In) ⟨100⟩ 120K

Sc = 0.5 Sr		Sc = 0.75 Sr	
Depth (um)	Chi (%)	Depth (um)	Chi (%)
0.08	2.3	0.093	2.28
0.21	2.6	0.184	2.58
0.34	3.2	0.297	3.14
0.47	3.6	0.409	3.59
0.59	4.4	0.519	4.35
0.72	5.0	0.627	4.95
0.84	6.0	0.734	5.87
0.96	6.4	0.840	6.30
1.08	7.0	0.943	6.85
1.19	7.9	1.05	7.78
1.31	8.8	1.15	8.59
1.42	10.1	1.24	9.78
1.53	11.0	1.34	10.69
1.64	12.1	1.44	11.71
1.75	13.3	1.53	12.81
1.85	14.6	1.62	13.96
1.96	15.9	1.72	15.14
2.06	17.0	1.81	16.22
2.16	18.5	1.89	17.53
2.26	19.4	1.98	18.36
2.36	21.0	2.06	19.77
2.45	22.3	2.15	20.93
2.54	23.5	2.23	21.96
2.64	24.7	2.31	23.02
2.72	26.5	2.39	24.54
2.81	27.5	2.46	25.44
2.90	29.4	2.54	26.99
2.98	31.0	2.61	28.39
3.06	33.1	2.68	30.15
3.14	34.0	2.75	30.91
3.22	35.3	2.82	31.96
3.30	37.0	2.89	33.38
3.37	38.0	2.96	34.09
3.45	39.8	3.02	35.58

Dechanneling Fraction Cu(.01In) ⟨100⟩ 200K

Sc = 0.5 Sr		Sc = 0.75 Sr	
Depth (um)	Chi (%)	Depth (um)	Chi (%)
0.08	3.0	0.093	3.02
0.21	4.0	0.184	4.00
0.34	4.9	0.297	4.86
0.47	5.4	0.409	5.39
0.59	6.3	0.519	6.21
0.72	8.0	0.627	7.87
0.84	8.8	0.734	8.64
0.96	10.2	0.840	10.07
1.08	11.0	0.943	10.80
1.19	12.6	1.05	12.36
1.31	14.0	1.15	13.70
1.42	15.7	1.24	15.27
1.53	17.3	1.34	16.71
1.64	18.8	1.44	18.12
1.75	20.8	1.53	20.01
1.85	22.7	1.62	21.77
1.96	24.3	1.72	23.23
2.06	26.4	1.81	25.09
2.16	27.9	1.89	26.45
2.26	29.8	1.98	28.17
2.36	31.8	2.06	29.95
2.45	33.4	2.15	31.37
2.54	35.2	2.23	32.88
2.64	37.3	2.31	34.70
2.72	40.4	2.39	37.45
2.81	40.0	2.46	37.03
2.90	42.6	2.54	39.25
2.98	45.1	2.61	41.40
3.06	46.0	2.68	42.11
3.14	47.9	2.75	43.71
3.22	49.8	2.82	45.20
3.30	51.8	2.89	46.89
3.37	51.9	2.96	46.84
3.45	55.1	3.02	49.45

Dechanneling Fraction Cu(.01In) ⟨100⟩ 280K

Sc = 0.5 Sr		Sc = 0.75 Sr	
Depth (um)	Chi (%)	Depth (um)	Chi (%)
0.08	3.9	0.093	3.86
0.21	5.3	0.184	5.26
0.34	6.5	0.297	6.47
0.47	7.6	0.409	7.56
0.59	9.1	0.519	9.06
0.72	10.4	0.627	10.25
0.84	12.2	0.734	12.05
0.96	13.6	0.840	13.33
1.08	15.3	0.943	15.03
1.19	17.7	1.05	17.30
1.31	19.4	1.15	18.94
1.42	22.2	1.24	21.53
1.53	24.3	1.34	23.39
1.64	26.0	1.44	25.14
1.75	29.2	1.53	28.05
1.85	31.7	1.62	30.39
1.96	33.8	1.72	32.30
2.06	35.9	1.81	34.16
2.16	38.7	1.89	36.72
2.26	40.5	1.98	38.25
2.36	42.5	2.06	40.07
2.45	45.1	2.15	42.35
2.54	45.8	2.23	42.92
2.64	48.0	2.31	44.87
2.72	49.5	2.39	46.10
2.81	51.0	2.46	47.39
2.90	53.7	2.54	49.64
2.98	54.7	2.61	50.46
3.06	58.1	2.68	53.34
3.14	59.9	2.75	54.79
3.22	60.5	2.82	55.27
3.30	63.8	2.89	57.95
3.37	63.8	2.96	57.81
3.45	66.8	3.02	60.25

September
2.0 MeV proton backscattering spectrum on Cu.
Gr2 Sp2 ⟨110⟩ tilt 16.33 280K 1.0 uC

30	2772	2759	2664	2670	2730	2746	2761	2789	2826	2787
40	2876	2735	2741	2772	2704	2723	2786	2838	2741	2805
50	2843	2817	2805	2786	2706	2702	2742	2711	2735	2787
60	2819	2714	2776	2823	2689	2741	2670	2665	2696	2707
70	2634	2697	2677	2631	2726	2687	2731	2639	2697	2571
80	2664	2613	2559	2628	2622	2565	2604	2490	2552	2540
90	2554	2628	2482	2552	2489	2538	2428	2514	2454	2445
100	2363	2328	2381	2348	2292	2374	2330	2245	2315	2234
110	2274	2166	2209	2190	2188	2046	2086	2106	2106	2023
120	2071	2053	2024	1968	1967	1999	1888	1872	1827	1849
130	1822	1795	1864	1776	1808	1656	1682	1590	1626	1662
140	1605	1522	1506	1482	1487	1458	1417	1461	1357	1293
150	1282	1279	1311	1174	1273	1134	1225	1106	1024	1034
160	1021	1058	977	1001	951	909	911	873	802	817
170	813	739	700	715	863	603	620	599	535	550
180	530	453	503	425	416	448	368	370	344	331
190	307	281	262	255	233	195	182	145	154	155
200	136	182	127	9	0					

2.0 MeV proton backscattering spectrum on Cu.
Gr3 Sp3 ⟨100⟩ tilt 31.75 280K 1.0 uC

30	3725	3778	3811	3785	3808	3809	3803	3823	3845	3846
40	3809	3735	3845	3724	3803	3831	3796	3932	3870	3978
50	3791	3858	3968	3957	3906	3849	3876	3925	3822	3864
60	3897	3870	3950	3902	3834	3834	3778	3841	3872	3858
70	3911	3899	3908	3921	3862	3914	3954	3810	3918	3861
80	3884	3872	3859	3835	3837	3800	3808	3697	3861	3787
90	3833	3811	3803	3669	3791	3662	3701	3557	3700	3652
100	3675	3599	3712	3678	3653	3612	3626	3567	3476	3602
110	3500	3542	3457	3526	3447	3326	3482	3427	3388	3401
120	3234	3346	3331	3307	3241	3135	3228	3167	3029	3019
130	3072	3037	3020	2911	2979	2883	2842	2893	2812	2812
140	2831	2800	2700	2624	2705	2653	2658	2511	2494	2455
150	2429	2394	2392	2409	2275	2230	2230	2147	2195	2106
160	2075	2001	2033	1962	1904	1835	1894	1838	1733	1725
170	1659	1560	1452	1464	1420	1358	1308	1282	1239	1209
180	1122	1077	1058	962	949	931	895	789	739	746
190	691	604	573	544	458	430	362	332	328	264
200	249	296	103	6	7					

2.0 MeV proton backscattering spectrum on Cu.
Gr4 Sp4 <100> tilt 31.78 56K 1.0 uC

30	2190	2218	2229	2291	2296	2301	2213	2242	2273	2269
40	2234	2235	2271	2233	2215	2286	2278	2246	2317	2251
50	2269	2283	2227	2230	2255	2168	2139	2175	2239	2248
60	2135	2188	2285	2168	2217	2142	2230	2176	2155	2188
70	2163	2167	2191	2117	2123	2160	2118	2116	2114	2085
80	2111	2090	2067	2019	2032	1976	1981	2025	2034	1873
90	2004	1994	1841	1828	1912	1887	1849	1888	1761	1844
100	1816	1777	1820	1719	1792	1756	1736	1695	1760	1762
110	1668	1676	1565	1614	1552	1571	1558	1550	1550	1484
120	1524	1460	1472	1406	1463	1391	1401	1373	1345	1340
130	1267	1319	1239	1212	1176	1214	1165	1210	1145	1108
140	1130	1063	1058	1001	947	973	973	926	871	920
150	910	807	822	872	773	765	750	705	690	709
160	655	673	657	586	601	558	551	479	499	499
170	447	460	467	442	394	354	376	344	323	312
180	330	306	257	250	240	225	216	207	190	169
190	160	135	140	130	130	131	97	93	89	90
200	81	130	88	8	1					

2.0 MeV proton backscattering spectrum on Cu.
Gr5 Sp5 <110> tilt 16.33 56K 1.0 uC

30	1297	1283	1305	1312	1325	1205	1264	1272	1251	1312
40	1233	1231	1242	1211	1190	1240	1273	1210	1262	1209
50	1203	1181	1241	1260	1235	1178	1236	1197	1155	1225
60	1219	1191	1245	1198	1160	1119	1191	1126	1140	1153
70	1126	1085	1115	1137	1152	1066	1095	1114	1095	1050
80	1050	1071	1051	1067	1070	993	1035	988	1080	994
90	914	968	993	958	939	914	933	958	870	912
100	880	819	879	881	847	841	839	804	789	786
110	830	827	728	784	734	776	670	741	709	712
120	694	625	673	695	607	646	661	639	602	561
130	591	578	514	530	543	557	551	490	484	495
140	477	466	493	441	428	426	402	426	398	388
150	401	371	389	375	351	336	311	313	317	317
160	274	256	267	274	252	274	246	228	229	223
170	199	206	195	200	178	150	163	152	158	157
180	135	119	103	131	100	115	90	90	84	85
190	94	69	87	73	59	62	72	52	45	39
200	49	131	32	1	0					

2.0 MeV proton backscattering spectrum on Cu.
Gr6 Sp6 <110> tilt 16.33 166K 1.0 uC

30	2116	2152	2101	2134	2197	2186	2216	2159	2156	2230
40	2205	2115	2190	2196	2135	2110	2096	2188	2214	2183
50	2157	2211	2210	2173	2157	2127	2166	2099	2137	2120
60	2151	2106	2132	2110	2173	2138	2107	2101	2117	2044
70	2116	2075	2056	2096	2098	1991	1967	2058	1878	1945
80	1957	2084	1965	1900	1906	1899	1941	1913	1822	1916
90	1848	1834	1800	1797	1827	1808	1778	1712	1779	1850
100	1747	1702	1694	1686	1713	1674	1681	1684	1541	1613
110	1572	1610	1547	1512	1541	1516	1469	1463	1381	1431
120	1486	1401	1415	1367	1342	1330	1390	1269	1272	1284
130	1229	1174	1187	1205	1174	1105	1151	1159	1156	991
140	1069	952	999	1001	955	951	941	921	878	833
150	857	799	846	791	748	718	738	703	652	658
160	588	620	629	623	617	573	518	499	448	493
170	435	419	424	403	400	327	336	336	319	315
180	280	273	254	239	232	223	190	187	188	197
190	174	150	132	144	108	106	102	96	85	80
200	97	129	52	2	0					

2.0 MeV proton backscattering spectrum on Cu.
Gr7 Sp7 <100> tilt 31.77 170K 1.0 uC

30	3322	3285	3347	3293	3367	3230	3374	3348	3463	3370
40	3343	3327	3399	3357	3326	3388	3328	3292	3388	3486
50	3328	3427	3466	3396	3370	3340	3363	3428	3341	3333
60	3430	3459	3407	3452	3360	3415	3320	3384	3369	3349
70	3493	3467	3267	3291	3303	3358	3267	3195	3281	3305
80	3328	3308	3264	3324	3242	3143	3297	3200	3273	3144
90	3148	3222	3194	3074	3194	3134	3196	3052	2985	2995
100	3024	3011	3021	3055	3016	2918	2993	3005	2902	2891
110	2890	2943	2908	2872	2820	2754	2767	2721	2807	2743
120	2714	2679	2572	2561	2626	2573	2540	2506	2550	2421
130	2415	2392	2454	2407	2376	2266	2275	2312	2185	2214
140	2179	2205	2133	2143	1991	1931	2022	1909	1868	1861
150	1821	1752	1733	1775	1764	1664	1629	1592	1531	1485
160	1448	1407	1401	1395	1329	1309	1266	1265	1132	1172
170	1196	1128	1087	1040	980	970	908	847	849	868
180	727	714	702	645	658	601	590	557	454	470
190	403	384	375	338	291	286	230	234	202	163
200	151	213	77	9	2					

2.0 MeV proton backscattering spectrum on Cu.
Gr7 Sp8 random rotating tilt 20.00 (rot. 90-180) 1.0 uC

30	436	500	533	494	483	523	445	514	491	466
40	474	493	463	467	467	506	497	530	537	492
50	489	544	501	486	507	532	483	522	499	525
60	513	499	495	531	513	533	515	541	569	540
70	516	497	545	558	513	538	507	521	542	505
80	493	591	534	553	501	557	562	529	504	499
90	552	537	513	543	498	525	516	569	499	506
100	538	533	513	522	535	576	543	536	572	483
110	560	507	565	564	530	554	565	548	512	563
120	553	556	501	537	500	551	516	506	518	536
130	532	525	524	554	527	546	510	542	528	519
140	550	564	511	513	505	547	537	562	553	523
150	562	528	543	535	525	507	535	520	534	528
160	541	532	510	527	518	496	506	518	514	567
170	485	523	417	507	500	470	525	500	561	496
180	510	473	520	511	506	545	495	496	471	481
190	485	486	474	454	436	516	471	532	470	486
200	490	345	51	2	1					

Dechanneling Fraction Cu#2 $\langle 110 \rangle$ 56K

Sc = 0.5 Sr		Sc = 0.75 Sr	
Depth (um)	Chi (%)	Depth (um)	Chi (%)
0.160	0.92	0.140	0.92
0.556	1.36	0.487	1.36
0.945	1.83	0.829	1.82
1.33	2.32	1.16	2.31
1.70	3.07	1.49	3.03
2.07	3.69	1.82	3.64
2.44	4.41	2.14	4.34
2.79	5.51	2.45	5.41
3.14	6.15	2.75	6.02
3.48	7.25	3.05	7.07
3.82	8.02	3.35	7.80
4.15	8.97	3.64	8.69
4.47	9.99	3.92	9.65
4.78	11.36	4.19	10.93
5.21	13.21	4.57	12.65
5.51	14.04	4.83	13.41
5.80	15.29	5.09	14.55
6.09	16.70	5.34	15.84
6.37	17.53	5.58	16.58
6.64	18.99	5.82	17.90
6.90	20.53	6.05	19.27
7.16	21.44	6.27	20.07
7.41	23.22	6.49	21.65
7.65	24.40	6.70	22.67
7.88	25.35	6.91	23.50
8.11	26.59	7.11	24.56
8.33	27.15	7.30	25.02
8.55	29.89	7.49	25.39
8.75	29.89	7.67	25.35
8.95	31.45	7.84	28.67
9.14	32.11	8.01	29.20
9.33	33.33	8.17	30.22
9.51	34.56	8.33	31.23
9.68	36.79	8.48	33.09

Dechanneling Fraction Cu#2 ⟨110⟩ 170K

Sc = 0.5 Sr		Sc = 0.75 Sr	
Depth (um)	Chi (%)	Depth (um)	Chi (%)
0.160	1.82	0.140	1.82
0.556	2.52	0.487	2.51
0.945	3.87	0.829	3.85
1.33	4.67	1.16	4.63
1.70	6.24	1.49	6.17
2.07	7.91	1.82	7.80
2.44	9.34	2.14	9.19
2.79	12.51	2.45	12.26
3.14	12.85	2.75	12.57
3.48	15.41	3.05	15.02
3.82	17.38	3.35	16.89
4.15	20.19	3.64	19.54
4.47	22.15	3.92	21.38
4.78	24.28	4.19	23.37
5.21	27.76	4.57	26.60
5.51	29.85	4.83	28.52
5.80	30.55	5.09	29.14
6.09	33.05	5.34	31.41
6.37	35.20	5.58	33.35
6.64	37.45	5.82	35.37
6.90	39.67	6.05	37.34
7.16	40.50	6.27	38.05
7.41	42.75	6.49	40.03
7.65	44.43	6.70	41.48
7.88	45.29	6.91	42.20
8.11	48.83	7.11	45.29
8.33	48.97	7.30	45.35
8.55	52.07	7.49	48.02
8.75	52.11	7.67	47.99
8.95	55.08	7.84	50.51
9.14	54.58	8.01	50.01
9.33	58.21	8.17	53.09
9.51	58.59	8.33	53.33
9.68	58.17	8.48	52.89

Dechanneling Fraction Cu#2 ⟨110⟩ 280K

Sc = 0.5 Sr		Sc = 0.75 Sr	
Depth (um)	Chi (%)	Depth (um)	Chi (%)
0.160	3.09	0.140	3.08
0.556	4.74	0.487	4.73
0.945	6.81	0.829	6.77
1.33	8.75	1.16	8.68
1.70	10.89	1.49	10.77
2.07	13.84	1.82	13.65
2.44	16.46	2.14	16.19
2.79	19.59	2.45	19.22
3.14	21.24	2.75	20.79
3.48	24.98	3.05	24.37
3.82	26.89	3.35	26.18
4.15	30.44	3.64	29.53
4.47	32.81	3.92	31.76
4.78	36.54	4.19	35.24
5.21	39.69	4.57	38.14
5.51	42.59	4.83	40.81
5.80	43.16	5.09	41.31
6.09	46.34	5.34	44.20
6.37	48.85	5.58	46.46
6.64	50.73	5.82	48.12
6.90	54.48	6.05	51.48
7.16	55.96	6.27	52.76
7.41	56.58	6.49	53.27
7.65	58.28	6.70	54.72
7.88	60.51	6.91	56.65
8.11	61.08	7.11	57.09
8.33	61.26	7.30	57.18
8.55	66.16	7.49	61.43
8.75	65.39	7.67	60.67
8.95	68.91	7.84	63.67
9.14	68.69	8.01	63.39
9.33	72.77	8.17	66.85
9.51	72.61	8.33	66.61
9.68	71.95	8.48	65.96

Dechanneling Fraction Cu#2 <100> 56K

Sc = 0.5 Sr		Sc = 0.70 Sr	
Depth (um)	Chi (%)	Depth (um)	Chi (%)
0.160	1.81	0.144	1.80
0.556	2.65	0.500	2.64
0.945	3.59	0.850	3.57
1.33	4.81	1.19	4.78
1.70	6.62	1.53	6.56
2.07	8.54	1.86	8.44
2.44	9.70	2.19	9.57
2.79	12.20	2.51	12.00
3.14	13.99	2.82	13.73
3.48	16.33	3.13	15.99
3.82	18.02	3.43	17.60
4.15	20.59	3.73	20.06
4.47	23.36	4.02	22.69
4.78	25.09	4.30	24.32
5.21	29.07	4.69	28.06
5.51	31.17	4.95	30.02
5.80	32.45	5.21	31.20
6.09	34.35	5.47	32.95
6.37	37.50	5.72	35.86
6.64	39.09	5.96	37.30
6.90	41.01	6.20	39.04
7.16	42.79	6.43	40.64
7.41	44.42	6.66	42.10
7.65	46.78	6.87	44.22
7.88	49.12	7.09	46.30
8.11	50.25	7.29	47.28
8.33	50.63	7.49	47.57
8.55	53.34	7.68	49.97
8.75	53.55	7.86	50.09
8.95	56.67	8.04	52.83
9.14	57.43	8.21	53.44
9.33	60.05	8.38	55.72
9.51	60.22	8.54	55.80
9.68	60.81	8.70	56.25

Dechanneling Fraction Cu#2 ⟨100⟩ 170K

Sc = 0.5 Sr		Sc = 0.70 Sr	
Depth (um)	Chi (%)	Depth (um)	Chi (%)
0.160	3.58	0.144	3.58
0.556	6.42	0.500	6.40
0.945	9.21	0.850	9.17
1.33	12.90	1.19	12.81
1.70	16.70	1.53	16.55
2.07	20.93	1.86	20.68
2.44	23.72	2.19	23.41
2.79	27.65	2.51	27.22
3.14	30.13	2.82	29.62
3.48	35.39	3.13	34.68
3.82	37.23	3.43	36.44
4.15	41.75	3.73	40.75
4.47	44.73	4.02	43.59
4.78	48.63	4.30	47.27
5.21	52.75	4.69	51.12
5.51	55.12	4.95	53.33
5.80	56.98	5.21	55.03
6.09	60.42	5.47	58.22
6.37	61.95	5.72	59.60
6.64	64.99	5.96	62.37
6.90	66.89	6.20	64.08
7.16	69.20	6.43	66.15
7.41	70.33	6.66	67.13
7.65	72.56	6.87	69.12
7.88	73.73	7.09	70.12
8.11	76.21	7.29	72.30
8.33	75.42	7.49	71.52
8.55	80.60	7.68	76.12
8.75	79.17	7.86	74.77
8.95	82.36	8.04	77.55
9.14	81.41	8.21	76.62
9.33	86.89	8.38	81.43
9.51	85.66	8.54	80.24
9.68	85.90	8.70	80.37

Dechanneling Fraction Cu#2 ⟨100⟩ 280K

Sc = 0.5 Sr		Sc = 0.70 Sr	
Depth (um)	Chi (%)	Depth (um)	Chi (%)
0.160	5.83	0.144	5.83
0.556	10.04	0.500	10.01
0.945	15.11	0.850	15.04
1.33	19.19	1.19	19.06
1.70	24.33	1.53	24.12
2.07	29.65	1.86	29.33
2.44	34.64	2.19	34.19
2.79	39.00	2.51	38.42
3.14	42.94	2.82	42.23
3.48	46.73	3.13	45.88
3.82	49.12	3.43	48.16
4.15	54.64	3.73	53.43
4.47	56.99	4.02	55.65
4.78	59.91	4.30	58.39
5.21	64.69	4.69	62.87
5.51	68.46	4.95	66.39
5.80	69.57	5.21	67.39
6.09	72.19	5.47	69.80
6.37	74.44	5.72	71.85
6.64	77.84	5.96	74.96
6.90	78.55	6.20	75.56
7.16	81.60	6.43	78.31
7.41	81.76	6.66	78.40
7.65	83.53	6.87	79.95
7.88	86.22	7.09	82.34
8.11	86.66	7.29	82.67
8.33	83.68	7.49	79.90
8.55	89.60	7.68	85.17
8.75	89.14	7.86	84.68
8.95	92.46	8.04	87.58
9.14	91.39	8.21	86.54
9.33	95.89	8.38	90.48
9.51	95.16	8.54	89.73
9.68	95.10	8.70	89.59